Remote Sensing of Environment 305 (2024) 114082

Contents lists available at ScienceDirect

Remote Sensing of Environment

journal homepage: www.elsevier.com/locate/rse

Spectra-phenology integration for high-resolution, accurate, and scalable mapping of foliar functional traits using time-series Sentinel-2 data

Shuwen Liu [a], Zhihui Wang [b], Ziyu Lin [a], Yingyi Zhao [a], Zhengbing Yan [c], Kun Zhang [a], Marco Visser [d], Philip A. Townsend [e], Jin Wu [a,f,*]

[a] School of Biological Sciences, The University of Hong Kong, Pokfulam, Hong Kong, China
[b] Guangdong Provincial Key Laboratory of Remote Sensing and Geographical Information System, Guangdong Open Laboratory of Geospatial Information Technology and Application, Guangzhou Institute of Geography, Guangdong Academy of Sciences, Guangzhou 510070, China
[c] State Key Laboratory of Vegetation and Environmental Change, Institute of Botany, Chinese Academy of Sciences, Xiangshan, Beijing, China
[d] Institute of Environmental Sciences, Leiden University, Einsteinweg 2, 2333 CC Leiden, The Netherlands
[e] Department of Forest and Wildlife Ecology, University of Wisconsin-Madison, 1630 Linden Drive, Madison, WI 53706, USA
[f] Institute of Climate and Carbon Neutrality, The University of Hong Kong, Pokfulam, Hong Kong, China

ARTICLE INFO

Editor name: Jing M. Chen

Keywords:
Plant traits
Sentinel-2
Time-series
NEON
Machine learning
Leaf economics spectrum

ABSTRACT

Foliar functional traits are essential for understanding plant adaptation strategies and ecosystem function. Due to limited *in-situ* observational data, there is a growing interest in upscaling these traits from field sites to regional and global levels. However, limitations persist: (1) global/national scale upscaling that relies on plant functional type (PFT) maps, environmental variables or coarse resolution multispectral images, which fail to capture local-scale trait variability; (2) airborne imaging spectroscopy that enables high-resolution and accurate mapping but is restricted to site scale and is costly; and (3) multispectral satellites like Sentinel-2 that offer global coverage but have limited spectral bands and resolution. While previous research has demonstrated the connection between traits and vegetation phenology, our study seeks to build upon this foundation by further exploring the integration of phenological information for large-scale trait prediction. We examined the integration of Sentinel-2 data with its time series (for phenology information) to map 12 foliar functional traits across 14 National Ecological Observatory Network (NEON) sites in the eastern United States. Our results show that time-series Sentinel-2 models effectively capture the variance in these 12 traits (R^2 = 0.60–0.80) when compared with benchmark trait data generated by state-of-the-art airborne imaging spectroscopy. The models adequately capture considerable trait variations observed within sites and PFTs. Our approach outperforms existing methods that rely on environmental variables, or a single Sentinel-2 image as predictors across examined NEON sites in eastern United States. Interestingly, including environmental variables in our models does not significantly improve predictive power. Further analysis reveals that a 'fast-slow' principal axis predominantly explains the covariation in Enhanced Vegetation Index amplitude (a proxy for leaf longevity), leaf mass per area, and leaf nitrogen content across PFTs. This finding highlights the importance of incorporating phenological information for trait mapping and suggests a potential mechanism underlying these spectra-based models. Our proposed method, which simultaneously achieves high accuracy, large-scale scalability, and high spatial resolution, represents a promising avenue for future global trait mapping. Validation on a larger scale to fully realize its potential in addressing fundamental ecological questions will be a key future focus.

1. Introduction

Plant functional traits represent multiple inter-connected characteristics of plants that are important to growth, structure and stress tolerance. Prediction of changes in ecosystem function in response to climate change based on suites of plant traits rather than species identity is of great interest in ecological studies due to the large number of species present on Earth (Funk et al., 2017; Chacón-Labella et al., 2022). Functional traits encompass variations in morphological, physiological, and phenological properties (Violle et al., 2007), reflecting fundamental

* Corresponding author at: School of Biological Sciences, The University of Hong Kong, Pokfulam Road, Hong Kong Special Administrative Region, China.
E-mail address: jinwu@hku.hk (J. Wu).

https://doi.org/10.1016/j.rse.2024.114082
Received 21 October 2023; Received in revised form 3 February 2024; Accepted 21 February 2024
Available online 26 February 2024

processes related to plants' evolutionary history (Cavender-Bares et al., 2022; Furey and Tilman, 2023; Yan et al., 2023), evolutionary strategy (Wright et al., 2004; Díaz et al., 2016), and adaptability to changing environmental conditions (Bjorkman et al., 2018; Myers-Smith et al., 2019). These traits, together with their spatial variation (functional diversity), significantly drive ecosystem productivity (Reich, 2012; Tilman et al., 2014), stability (Liang et al., 2022), and the resulting services (IPBES, 2019), and therefore have been utilized to assess the fate of ecosystems in the context of climate change and other perturbations. Earth system modelers employ functional traits to parameterize vegetation, aiming to reduce prediction uncertainty in carbon cycles (Rogers et al., 2017; Walker et al., 2017). Since leaf morphology, pigmentation, and biochemical components, along with plant canopy structure, are dominant signals observed in spectral imaging, remote sensing provides the ability for large-scale characterization of plant traits (Féret et al., 2021; Gamon et al., 2019; Liu et al., 2023).

Trait data collection is typically performed through field sampling, but this process is often labor-intensive and restricted to a narrow geographical scope and selected species. As a result, significant efforts have been made to aggregate plant trait data from previous studies, resulting in the establishment of the TRY database (Kattge et al., 2020). However, the species sampled in the TRY database, which include plant trait data, account for only 5% of the currently identified vascular plant species on Earth for leaf mass per area (LMA) and 3.4% for leaf nitrogen content (Kattge et al., 2020). Given the logistical constraints of characterizing spatial-wise trait variation through field sampling, there has been growing interest in exploring trait upscaling at landscape (Wessman et al., 1988; Martin et al., 2008; Singh et al., 2015; Asner et al., 2015; Wang et al., 2020), regional (Asner et al., 2017; Aguirre-Gutiérrez et al., 2021; Loozen et al., 2020; Wallis et al., 2019) and global scales (Boonman et al., 2020; Butler et al., 2017; Madani et al., 2018; Moreno-Martínez et al., 2018; Schiller et al., 2021; Vallicrosa et al., 2022; van Bodegom et al., 2014). Although the motivations for these scaling studies were numerous, the approaches they used can generally be split into three categories: the PFT-based approach, the statistical modeling approach relying on environmental variables, and the remote sensing-based approach. In practice, these three categories of methods are also commonly used in combination.

Plant functional types (PFTs) describe species or more often communities of plants according to their dominant physiological, morphological and phenological characteristics, sometimes modified by climatic descriptors (Gitay and Noble, 1997; Kattge et al., 2020; Lavorel et al., 1997; Ustin and Gamon, 2010). Global PFT maps are generally derived from remote sensing. By integrating global PFT maps with trait data from databases, PFT-trait lookup tables can be constructed, facilitating the upscaling of field observations based on global PFT classifications (Lavorel et al., 1997). This method is advantageous due to its simplicity and ease of implementation, providing a level of detail that drives useful models at regional or global scales (Pacala and Kinzig, 2002). Another method is to use the PFT as a variable in statistical or machine learning modeling (*e.g.*, Butler et al., 2017). However, there is no general consensus regarding the inclusion or exclusion of specific functional traits in the PFT classification, resulting in its *ad hoc* application depending on the immediate purpose (Ustin and Gamon, 2010). More importantly, the local diversity of plant communities and the trait variation within a PFT in different environments is overlooked (Running et al., 1994; Wullschleger et al., 2014). Consequently, model parameters based on plant trait characteristics are limited by the classification of PFTs, resulting in a significant source of uncertainty in many terrestrial biosphere models (Reichstein et al., 2014; van Bodegom et al., 2014).

The environmental variable-driven statistical approach employs environmental factors (typically encompassing climate, soil, and terrain) in conjunction with field-observed trait data to develop a statistical model, which is then upscaled to a broader extent (reviewed by Dechant et al., 2023). Since these environmental variables have already been observed or interpolated at a global scale, these approaches allow for more straightforward upscaling of traits and offer greater detail compared to the PFT lookup table approach. However, due to the generally coarse spatial resolutions of macro-environmental variables, these methods produce low-resolution grid-cell-based global trait maps (0.008–0.5°, Dechant et al., 2023), leading to two associated challenges. The first challenge concerns the mismatch between field data and grid cells. Grid cells are significantly larger than the scale of *in-situ* observations, making it unlikely that the *in-situ* data accurately represents the entire grid cell (Asner et al., 2015; Dechant et al., 2023). The second challenge pertains to the implicit assumption that plant community traits are solely determined by environmental factors. Plant communities exhibit considerable intra-site trait variations due to biotic processes such as evolution, migration, disturbance, and biological interactions (Cavender-Bares et al., 2022). Consequently, environmental variable-driven statistical methods can only account for the abiotic regulatory factors influencing a trait. To address this challenge, some studies incorporated PFT or coarse resolution multispectral image information on top of the environmental variables used (Butler et al., 2017; Moreno-Martínez et al., 2018).

Airborne imaging spectroscopy is widely considered the preferred method for remote sensing-based trait upscaling. This approach is grounded in the fundamental biophysical principles underlying radiative transfer processes and plant spectroscopy, as it demonstrates a strong association between leaf/canopy reflectance spectra and their corresponding morphological, biochemical, and physiological properties (Curran, 1989; Elvidge, 1990; Kokaly et al., 2009). The advantages of airborne imaging spectroscopy include high spatial resolution (typically 1 m) and, more importantly, its ability to discern subtle differences in plant absorption and scattering properties (Wang et al., 2020). However, airborne imaging spectroscopy is expensive and because the resulting limited spatial coverage can only upscale *in-situ* observations to the landscape scales at which it is feasible to conduct airplane imaging. To date, the most extensive collection effort for airborne hyperspectral imagery for trait upscaling has gathered over 2 million ha of imagery (Asner et al., 2017) using the Carnegie Airborne Observatory (Asner et al., 2012). Nevertheless, this only covered 2.5% of the study area in the Peruvian Andes-Amazon region and required use of a random forest model with environmental data to cover the larger region of interest (Asner et al., 2017). Utilizing satellite remote sensing data can address the issue of large-scale scalability. Researchers have previously employed this method for invasive plant species identification using a combination of Sentinel-1 and Sentinel-2 (Kattenborn et al., 2019), as well as for experimental modeling of traits through spaceborne imaging spectroscopy data (Miraglio et al., 2023). For example, Aguirre-Gutiérrez et al. (2021) employed multispectral satellite imagery from Sentinel-2 to upscale *in-situ* trait data at pantropical region, and Moreno-Martínez et al. (2018) used multi-spectral information from MODIS for a similar purpose. However, the limited bands and lower spectral resolution of multispectral data compared to imaging spectrometers yield lower predictive accuracy than using imaging spectroscopy alone.

The suboptimal predictive accuracy of Aguirre-Gutiérrez et al. (2021) may also result from the underutilization of multispectral satellite observational techniques, particularly the phenological information embedded in satellite time-series observations. Globally, plant form and function are constrained by resource availability, leading to predictable relationships between phenological and physiological/biochemical characteristics of plants (Field, 1991; Reich et al., 1997; Ustin and Gamon, 2010; Whittaker, 1956; Wright et al., 2004). Empirical evidence from botanical garden experiments which maintain environmental consistency (Sporbert et al., 2022) and studies focus on the same PFT (Blumenthal et al., 2020; Liu et al., 2021), suggests that foliar traits and phenology remain coordinated. Consequently, it is plausible to hypothesize that integrating spectral-phenology information from satellite data has the potential to provide a trait upscaling method with high spatial resolution, large-scale scalability, and higher accuracy, thereby addressing the limitations of existing traits upscaling studies. Notably,

previous attempts have been made to integrate spectra-phenology for crop type (Cai et al., 2018) and forest species mapping (Grabska et al., 2020; Hemmerling et al., 2021), as well as trait estimation by Moreno-Martínez et al. (2018) using temporal information encoded in temporal metrics of VIs with MODIS time series. While MODIS data may not capture all the spectral features necessary to estimate specific traits, they can indirectly model differences between trait PFTs through temporal information. Despite these prior successes, the effectiveness of incorporating such temporal information in improving prediction accuracy, particularly for high-resolution Sentinel-2 data, has not been sufficiently examined.

The objective of this study is to investigate whether incorporating Sentinel-2 data and its time series (for phenological information) can provide an improved alternative approach for characterizing foliar functional traits. To evaluate the effectiveness of this approach, multi-dimensional foliar trait data capturing the natural variability of both intra-site and inter-site across large geographical extents is needed. For this purpose, we employed the trait maps generated by state-of-the-art airborne imaging spectroscopy across major ecosystem types of the National Ecological Observatory Network (NEON) in the United States (Wang et al., 2020). The combination of these high-quality trait maps with Sentinel-2 data represents a particularly innovative aspect of our work, as it enables us to develop and test a trait upscaling method with high spatial resolution, large-scale scalability, and higher accuracy. Note that although traits exhibit seasonal variation, we utilized traits at mid-season/peak greenness in this study, adhering to a consistent protocol commonly followed by plant ecologists. Consequently, we employ phenological information as supplementary context for predicting traits rather than predicting temporal variation in traits. Specifically, our study addresses the following research questions:

Q1. To what extent can the integration of spectral and phenological information from time-series Sentinel-2 data, combined with machine learning regression, capture the variation of multiple foliar functional traits in NEON sites?

Q2. How does our proposed method compare to existing approaches that utilize environmental variables or single Sentinel-2 images as predictor variables?

Q3. Which phenological stages and spectral bands are important predictors in the proposed trait prediction models based on time-series Sentinel-2 data?

2. Materials and methods

2.1. Materials

2.1.1. Selected NEON sites and associated foliar functional traits data

We utilized high spatial resolution maps of foliar functional traits (Wang et al., 2020) derived from an imaging spectrometer (426 bands between 380 and 2500 nm with a spectral sampling of 5 nm and 1 m spatial resolution; Kampe et al., 2010) mounted on the NEON Airborne Observation Platform (AOP). These maps were generated using partial least squares regression (PLSR) models, which were trained using airborne imaging spectroscopy data and >1000 individual-level *in-situ* foliar functional traits data from 18 NEON sites (Wang et al., 2020). Field campaigns at each site were conducted within two weeks of the NEON AOP flight, with approximately 90% of the field data collected in 2017 and the remaining 10% in 2016 (Wang et al., 2020). A total of 26 foliar traits were mapped across seven NEON domains, encompassing temperate and subtropical forests and grasslands in eastern America. We selected trait map data from 14 of the 18 sites for this study (Fig. 1 and Table S1) and excluded sites dominated by cropland ecosystems in Wang et al. (2020), due to the influence of human management on the temporal variation in reflectance. Two additional sites were also excluded because of insufficient NEON AOP flight coverage (<5 km^2).

The 14 selected sites spanned six NEON domains, with mean annual temperature (MAT) ranging from approximately 4.0 to 22.4°C and mean annul precipitation (MAP) ranging from around 817 to 1502 mm yr^{-1}. We utilized 12 foliar functional traits out of the 26 provided by Wang et al. (2020), as these traits are either ecologically important or directly

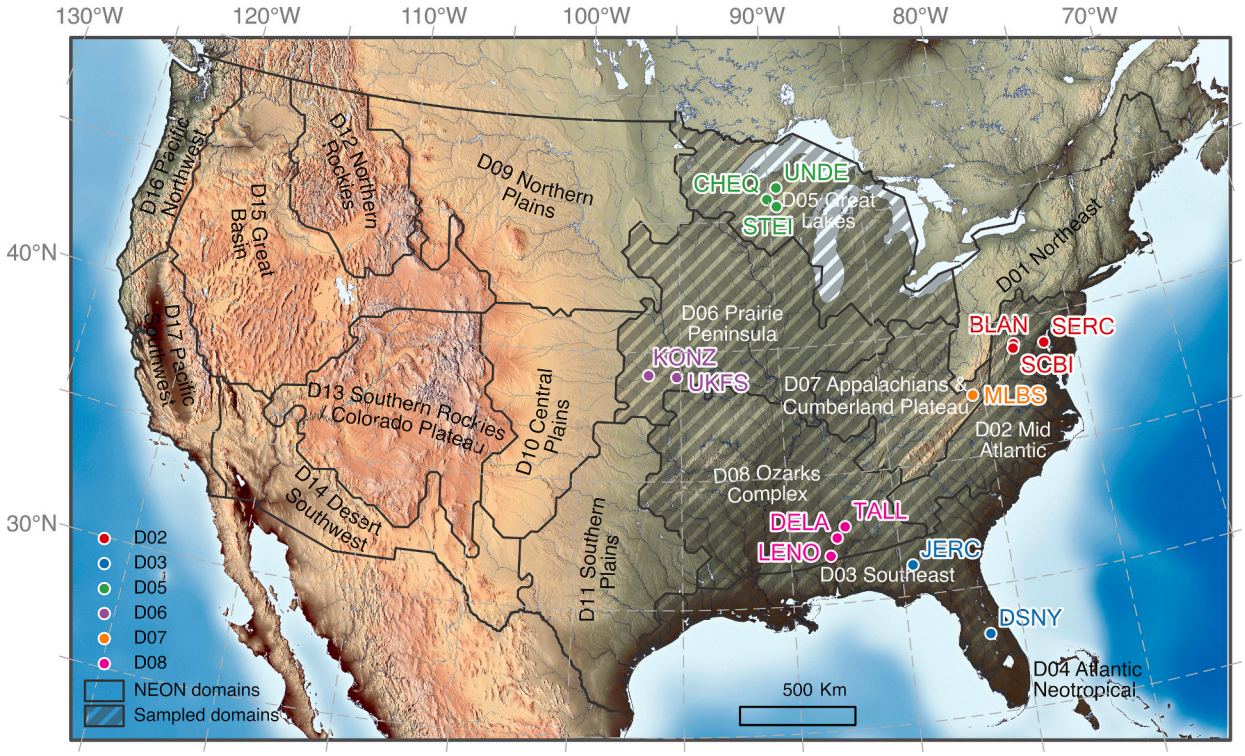

Fig. 1. 14 NEON sites selected for this study, spanning six NEON domains (marked as different colors). A terrain map renderied using the cross-blended hypsometric tints method is shown as the background.

associated with leaf reflectance spectra. These 12 foliar functional traits include carbon, carotenoids, cellulose, chlorophyll a + b, equivalent water thickness (EWT), lignin, LMA, nitrogen, nonstructural carbohydrates (NSC), phenolics, phosphorus, and potassium. Independent validation of PLSR models for these 12 functional traits demonstrated a coefficient of determination (R^2) ranging from 0.46 to 0.82 and a normalized root mean squared error (RMSE) ranging from 9.1% to 18% (Wang et al., 2020). We also considered the uncertainty of PLSR predictions by applying a threshold of 25% as suggested by Verrelst et al. (2016). Most of the trait maps in our selected sites – with the exception for Phenolics, Phosphorus, and Potassium - have >90% of pixels with high confidence (Fig. S1).

We downloaded maps of 12 selected functional traits and their predictive uncertainties from https://tinyurl.com/neontraits1. These downloaded trait maps are organized in a flight line format. Our first step was to mosaic the flight line trait maps and their corresponding uncertainties for each site. Next, we aggregated the trait maps and their respective uncertainties to a 10 m resolution to match that of the Sentinel-2 images. During the aggregation process, we used the Sentinel-2 images of each site to determine the cell location of the aggregated trait maps for that site (using ArcGIS built-in function 'aggregate' with geoprocessing tool 'snap raster'), ensuring proper co-alignment between the Sentinel-2 data and the trait maps. Lastly, we removed pixels with high predictive uncertainty (>25%) for the aggregated trait maps.

2.1.2. Sentinel-2 data with associated pre-processing, vegetation indices and canopy texture

To construct time-series features for modeling foliar functional traits, we utilized the Sentinel-2 Multispectral Instrument (MSI) Level-2 A data archived in the Google Earth Engine (GEE), operated by the European Space Agency (ESA). Our primary objective was to obtain a high-quality time-series-dense image collection containing reflectance data, vegetation indices and canopy texture variables (Fig. 2).

To achieve this, we first acquired all images from January 2019 to December 2022, totaling four years for each site. We selected images starting in 2019 since the ESA did not provide Level-2 A images for most sites before 2019. Next, we filtered out images with cloud coverage >75%. We then removed clouds, cloud shadows (based on Sentinel-2 cloud probability bands with a cloud probability >10%), and snow-contaminated pixels using a Normalized Difference Snow Index (NSDI) threshold (*i.e.*, NDSI >0) following Gascoin et al. (2019). We excluded all images from December to March for CHEQ, UNDE, and STEI sites, as these sites experienced snow for most of that period (Zhao et al., 2022). To further filter out non-vegetation pixels and pure branch pixels after complete leaf fall in winter, we also used an enhanced vegetation index (EVI) (Huete et al., 1997) threshold of 0.1. Subsequently, we minimized

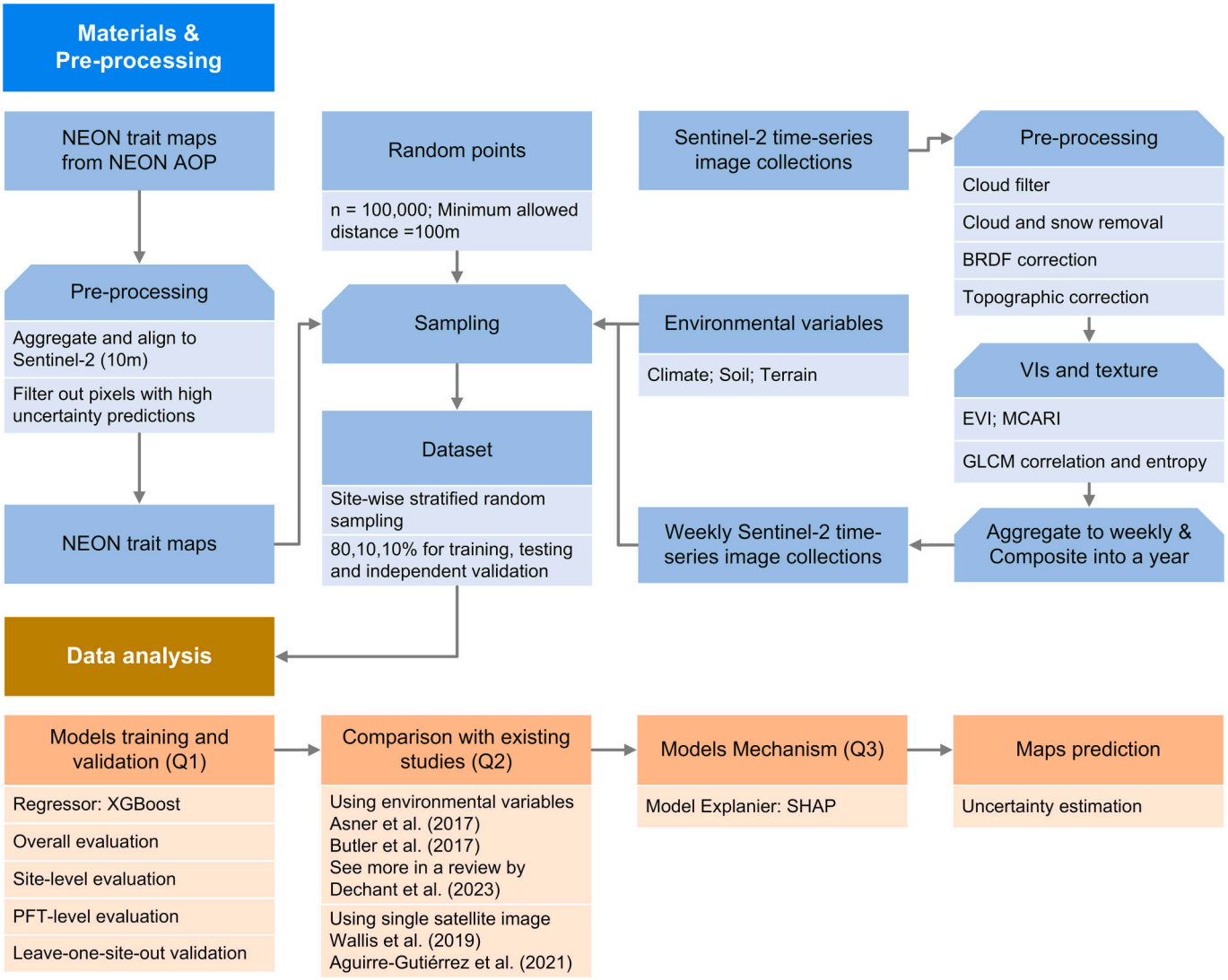

Fig. 2. A summary workflow diagram of materials with associated preprocessing and data analysis of this study.

the effects of solar and sensor view angle by applying a Bidirectional Reflectance Distribution Function (BRDF). We used BRDF kernel coefficients the same as harmonized Landsat and Sentinel-2 (HLS) product (Claverie et al., 2018). We performed a terrain-based path length correction algorithm to minimize topography effects following Yin et al. (2018). After preprocessing the Sentinel-2 images, we assigned each image a calendar week label to align images from different years to a consistent temporal scale. Subsequently, we synthesized images from four years into one-year weekly images by averaging all available images for each week, enabling us to obtain a denser time-series image collection for each site. The median value of the pixel-level time-series null rate for the derived Sentinel-2 image collections was 11.5%, and we excluded pixels with high time-series null rates (>60%) from subsequent analysis (Fig. S2).

With the time-series Sentinel-2 image collections, we next generated a range of features for building trait models. The first set of variables include the reflectance of B2, B3, B4, B5, B6, B7, B8, B8A, B11 and B12 bands of the Sentinel-2 MSI (Table 1). For bands with 20 m spatial resolution, we downscaled them to 10 m using the nearest neighbor resampling method. The second set of variables include the EVI and modified chlorophyll *a*bsorption in reflectance index (MCARI) (Daughtry et al., 2000), which track the greenness and chlorophyll content changes of the vegetation, respectively. The last set of variables are Grey Level Co-Occurrence Matrix (GLCM) based texture features (Haralick et al., 1973), which were calculated using a 9*9 pixel kernel window, as suggested by Aguirre-Gutiérrez et al. (2021). Specifically, the Entropy and Correlation variables based on the GLCM for EVI of each image were computed. Entropy measures the homogeneity level for a given area, while Correlation measures the probability of occurrence of specified pixel pairs across the image.

2.1.3. Environmental data

In this study, we characterized the topography, climate, and soil properties of our study sites using multiple environmental variables (Table S2). Specifically, elevation, slope, and aspect information were obtained from the Shuttle Radar Topography Mission (SRTM) digital elevation dataset at a spatial resolution of 30 m (Jarvis et al., 2008). We also employed the WorldClim2 product (Hijmans et al., 2005), which provides 19 bioclimatic variables with spatial resolution of 30 arcsec derived from monthly temperature and precipitation records. Moreover, major soil properties were assessed using 10 variables from the SoilGrids dataset (Poggio et al., 2021), focusing on maps for the top layer (0–5 cm). Additionally, we utilized soil moisture data from the SMAP-HydroBlocks (Vergopolan et al., 2021), a hyper-resolution satellite-based product covering the continental United States with a spatial resolution of 1 km. Based on this dataset, we calculated the mean annual surface soil moisture from 2015 to 2019, providing a climatological status for soil water content and covering the sampling period of *in-situ* trait data. Further details of each environmental variable are presented in Table S2.

Table 1
Spectral configuration of the 10 Sentinel-2 bands used in this study. Abbreviations for band names are in parentheses.

Spectral band	Band name	Center wavelength (nm)	Band width (nm)	Spatial resolution (m)
B2	Blue	490	65	10
B3	Green	560	35	10
B4	Red	665	30	10
B5	Red-edge 1 (RE 1)	705	15	20
B6	Red-edge 2 (RE 2)	740	15	20
B7	Red-edge 3 (RE 3)	783	20	20
B8	Near-infrared (NIR)	842	115	10
B8A	Near-infrared 2 (NIR 2)	865	20	20
B11	Short-wave infrared 1 (SWIR 1)	1610	90	20
B12	Short-wave infrared 2 (SWIR 2)	2190	180	20

2.1.4. Plant functional type data

In this study, PFT data were utilized to quantify the variation of traits in 14 NEON sites between and within PFTs. In addition, we used PFTs to evaluate the predictive capabilities of the models (see Section 2.2 below) at PFT-level. Finally, we employed PFT maps to exclude non-natural ecosystems from the analysis. PFTs were derived from the 2019 National Land Cover Database (NLCD), which is specifically designed for monitoring land cover and land cover changes across the United States (Dewitz, 2021). The NLCD land cover classification scheme clearly delineates distinct PFTs (see here for the full list of NLCD land cover classes). The primary PFTs identified at the selected 14 NEON sites include deciduous forest, mixed forest, evergreen forest, pasture/hay, grassland/herbaceous, shrub/scrub, and woody wetlands. We excluded non-vegetation land cover types and cultivated crops class from the data analysis. In addition, we omitted other PFTs that accounted for <1% of the total area of the studied NEON sites. Among all 14 NEON sites, deciduous forests, woody wetlands, mixed forests, and evergreen forests were the four largest PFTs in terms of area, collectively accounting for over 75% of the total area. The PFT composition at each site is summarized in Fig. S3.

2.2. Data analysis

2.2.1. Modeling foliar functional traits using time-series Sentinel-2 data

To prepare the dataset for addressing Q1, we employed a random point sampling method that reduces the original data volume for computational efficiency, while sampling the 12 functional trait maps and time-series Sentinel-2 images with associated VIs and textures (Section 2.1.2) at each site. We set the total number of random points across all study sites to 100,000, which is approximately 0.5% of the total number of pixels of the aggregated NEON AOP hyperspectral images for the 14 sites. Meanwhile, we set the minimum allowed distance between random points at 100 m to reduce spatial auto-correlation. The number of random points of each site was determined based on the NEON AOP coverage area of the sites, as described in Table S1. We excluded certain areas, such as patches of croplands or built-up areas, when delineating the analysis area. Due to the presence of null values or filtered pixels in both the functional trait maps and the time-series Sentinel-2 image collections, the average sample size of the final datasets prepared for the subsequent modeling step for 12 traits was 81,170. We refer to the models presented here as *Time-series RS* models (Table 2)

Table 2
Overview of models and associated features utilized in each modeling scenario. Environmental variables are detailed in Table S2. For *Single image RS* models, features were chosen from *Time-series RS* models based on the time point nearest to the trait sampling date at each site, as per Wang et al. (2020).

Models	Feature sets	Number of features
Time-series RS	Time-series Sentinel-2 reflectance, VIs and textures	728
Time-series RS + Env	Time-series Sentinel-2 reflectance, VIs and textures; Terrain, climate and soil	761
Env	Terrain, climate and soil	33
Env + PFT	Terrain, climate, soil and PFT	34
Single image RS	Sentinel-2 reflectance, VIs and textures	14

to distinguish them from the models that incorporate only environment variables and those that use a single Sentinel-2 image (see Section 2.2.2 below).

We utilized the extreme gradient boosting (XGBoost) regressor (Chen and Guestrin, 2016) to model and predict foliar functional traits from time-series Sentinel-2 image collections. XGBoost is an efficient, scalable gradient tree boosting algorithm widely used for machine learning tasks. It incorporates a unique technique for handling missing values through sparsity-aware split-finding during tree construction, making it particularly suitable for our tasks (missing values in satellite time-series data). The modeling process involved several steps. First, we divided the dataset into training, testing, and independent validation sets with an 80:10:10 ratio using site-stratified random sampling. Next, we optimized the hyperparameters of the XGBoost model to prevent overfitting and overcomplication. These hyperparameters can be classified into regularization (alpha, lambda), tree growth (max_depth, min_child_weight), and learning process (learning_rate, colsample_bytree, subsample), which contribute to model complexity control, overfitting prevention, and feature selection, respectively. We utilized the Bayesian optimization method to train the model on the training set and optimize hyperparameters by evaluating the RMSE on the testing set. Moreover, we used the early stopping technique to avoid overfitting. The hyperparameter optimization results of the model for each trait are presented in Table S3.

After optimization, we trained the model using the optimized hyperparameters and used the model to predict outcomes on the testing and independent validation sets. We assessed the model performance using the coefficient of determination (R^2), RMSE, mean absolute percentage error (MAPE) and normalized bias (nBias) as evaluation metrics. MAPE is calculated as the average of the absolute percentage differences between the predicted values and the actual values. nBias is calculated as the mean difference between the predicted and actual values, divided by the mean of the actual values. To interpret the impact of features on the model's predictions, we employed the Shapley Additive Explanations (SHAP) method (Lundberg et al., 2020). The SHAP method provides a unified measure of feature importance by attributing the output to each input feature, based on its contribution to the prediction in a fair and mathematically consistent manner. Model training and hyperparameter optimization were conducted using a Python environment on GPU nodes of the high-performance computing system of the University of Hong Kong. The 'optuna' package (Akiba et al., 2019) was employed for Bayesian optimization.

Furthermore, we conducted leave-one-site-out and leave-one-PFT-out validations, in which we successively kept samples from one site or one PFT for independent validation while utilizing samples from the remaining sites or PFTs for training. This method enabled us to evaluate if the *Time-series RS* models were overfitted and to determine the degree to which spectral-phenological features were generalizable for predicting in unseen sites and PFTs. Note that this was an additional experiment; results in the results section were primarily derived from the models trained through 80:10:10 split, rather than the leave-one-site-out or leave-one-PFT-out approaches, unless stated otherwise.

2.2.2. Comparing foliar trait models with different input

After evaluating the predictive accuracy of our *Time-series RS* models for traits, we further investigated how well two other modeling strategies (*i.e.*, including environmental variables or using a single multispectral image) contributed to trait characterizations for addressing Q2. To this end, we trained models using four feature sets, (1) environmental variables and the features used in *Time-series RS* models (*Time-series RS + Env* models), (2) environmental variables alone (*Env* models), (3) environmental variables and PFT classification from NLCD data (*Env + PFT* models), and (4) single-time Sentinel-2 images (*Single image RS* models) with same bands, vegetation indices and canopy texture used in *Time-series RS* models.

We used the same set of random points as Section 2.2.1 to sample a total of 33 environmental variables (as stated in Section 2.1.3) for the modeling of *Time-series RS + Env*, *Env* and *Env + PFT* models. For *Single image RS* models, we selected features based on the time closest to the trait sampling date at each site (Wang et al., 2020) from the *Time-series RS* models. For these three modeling scenarios, we employed the same training/testing/validation split, regression model, and model hyperparameter optimization methods as described in Section 2.2.1 for the *Time-series RS* models.

2.2.3. Mapping foliar functional traits using time-series RS models

For each trait, we applied the trained *Time-series RS* model (Section 2.2.1) to the preprocessed time-series Sentinel-2 image collections (Section 2.1.2) to generate trait maps. We employed quantile regression to obtain prediction intervals and prediction uncertainties, following (Landry et al., 2016). Quantile regression is a statistical method that estimates the relationship between a response variable and its explanatory variables across different quantiles of the response variable's distribution. Specifically, we used quantile regression to estimate the 5% and 95% confidence intervals for each predicted value and calculated the standard deviation of the predictions using these intervals. The relative uncertainties were computed as the ratio of standard deviation to the mean. We performed only minimal post-processing on the produced trait maps. We filtered out non-vegetated or sparsely vegetated pixels using a NDVI threshold of 0.3 and excluded pixels with high uncertainty by applying a relative uncertainty threshold of 0.25.

3. Results

3.1. The capability of spectra-phenology integration for charactering multi-dimensional foliar functional traits

All 12 traits from the 14 NEON sites exhibited a considerable range (Table S4). The coefficient of variation (CV) ranging from 0.21 to 0.43 except for carbon (CV = 0.05) (Table S4). We observed significant differences in traits between PFTs but also considerable variation within PFTs (Fig. 3). Taking LMA as an example, for deciduous trees, LMA had a mean value of 90.88 g m^{-2} with a CV of 0.32, while evergreen trees displayed a higher LMA (178.23 g m^{-2}, CV = 0.25) (Fig. 3g). Similar observations apply to all other foliar traits. For most foliar traits, we observed significantly different (higher or lower) trait values between tree PFTs (*e.g.*, deciduous forest, evergreen forest, and mixed and non-woody PFTs (*e.g.*, pasture/hay, grassland/herbaceous), with intermediate values for shrub/scrub and woody wetlands (Fig. 3). These phenomena are consistently observed across traits, except for EWT, LMA and Nitrogen, in which the evergreen forest PFT displays significantly higher or lower trait values compared with other PFTs (Fig. 3). Collectively, these results highlight the considerable trait variability in our data record stemming from various sources such as site, inter-PFT, and intra-PFT. The PFT-associated trait variations also vary greatly depending on the trait of interest.

We found that the spectra-phenology integration approach (*i.e.*, *Time-series RS* models) is capable of characterizing these traits. For overall evaluation, we observed that the *Time-series RS* models for all 12 traits performed almost identically on the test and independent validation sets in terms of both R^2 and RMSE (Table S5). This demonstrates that these models are not over-fitted, and exhibit good generalization ability. Consequently, we focused on describing the assessment results of the models on the independent validation set. R^2 value ranged from 0.60 (phenolics and phosphorous) to 0.80 (carbon, lignin and LMA) across all 12 foliar traits examined in this study (Fig. 4). MAPE values varied from 1.73% (carbon) to 16.94% (EWT), with 7 out of the 12 traits having a MAPE <10% (carbon, carotenoids, cellulose, chlorophyll *a* + b, lignin, nitrogen, NCS) (Fig. 4). The nBias for all traits was <0.5% (Fig. 4). The fitted lines of *Time-series RS* models' predictions at most sites closely align with the 1:1 line (Fig. 4).

The *Time-series RS* model demonstrates good performance at both

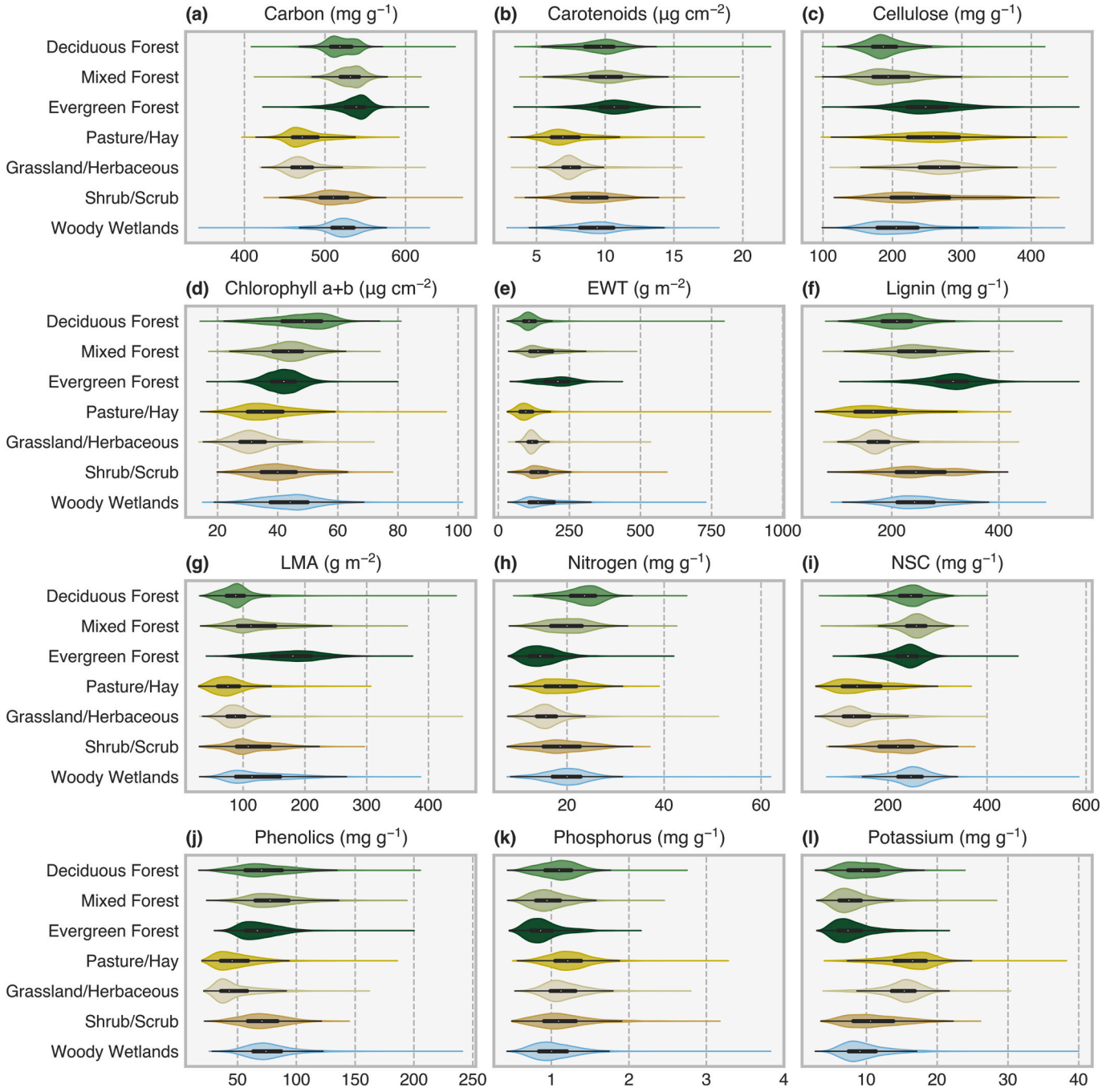

Fig. 3. Distribution of 12 foliar functional traits at PFT-level estimated by random points sampling. EWT, equivalent water thickness; LMA, leaf mass per area; NSC, nonstructural carbohydrate.

site-level (Fig. 5a and b) and PFT-level (Fig. 5c and d) evaluation, although there was a slight degradation compared to overall evaluation (Fig. 4). For the site-level evaluation, we observed that carbon has the highest mean site-level predictive power ($R^2 = 0.69$, Fig. 5a), followed by carotenoids, chlorophyll $a + b$, LMA, lignin, and potassium with $R^2 > 0.6$ (Fig. 5a), cellulose, EWT, NSC, and nitrogen with $R^2 > 0.5$ (Fig. 5a), and least in phenolics ($R^2 = 0.46$, Fig. 5a) and phosphorous ($R^2 = 0.42$, Fig. 5a). Similarly, we observed variation in the site-level evaluation across 14 sites, with DELA holding the highest mean predictive power ($R^2 = 0.69$, Fig. 5b), followed by UNDE and UKFs with $R^2 > 0.6$ (Fig. 5b), CHEQ, STEI, KONZ, SCBI, SERC, MLBS, TALL, LENO, JERC, DSNY with $R^2 > 0.5$ (Fig. 5b), and least in BLAN ($R^2 = 0.40$, Fig. 5b).

For the PFT-level evaluation, we observed that LMA has the highest mean predictive power across all PFTs ($R^2 = 0.69$, Fig. 5c), followed by carbon, cellulose, chlorophyll $a + b$, lignin, nitrogen and potassium with $R^2 > 0.6$ (Fig. 5c), carotenoids, EWT, NSC, and phosphorus with $R^2 > 0.5$ (Fig. 5c), and least in phenolics ($R^2 = 0.47$, Fig. 5c). Similarly, we observed considerable variation in the mean predictive power across all 7 PFTs, with deciduous forest PFT holding the highest mean predictive power ($R^2 = 0.67$, Fig. 5d), followed by woody wetlands and mixed forest ($R^2 = 0.64$, Fig. 5d), grassland/herbaceous ($R^2 = 0.59$, Fig. 5d), shrub/scrub and pasture/hay ($R^2 = 0.58$, Fig. 5d), and least in evergreen forest ($R^2 = 0.57$, Fig. 5d).

Our additional leave-one-site-out and leave-one-PFT-out validation indicated that *Time-series RS* models provided reasonable prediction accuracy for most traits even in sites or PFTs lacking training samples

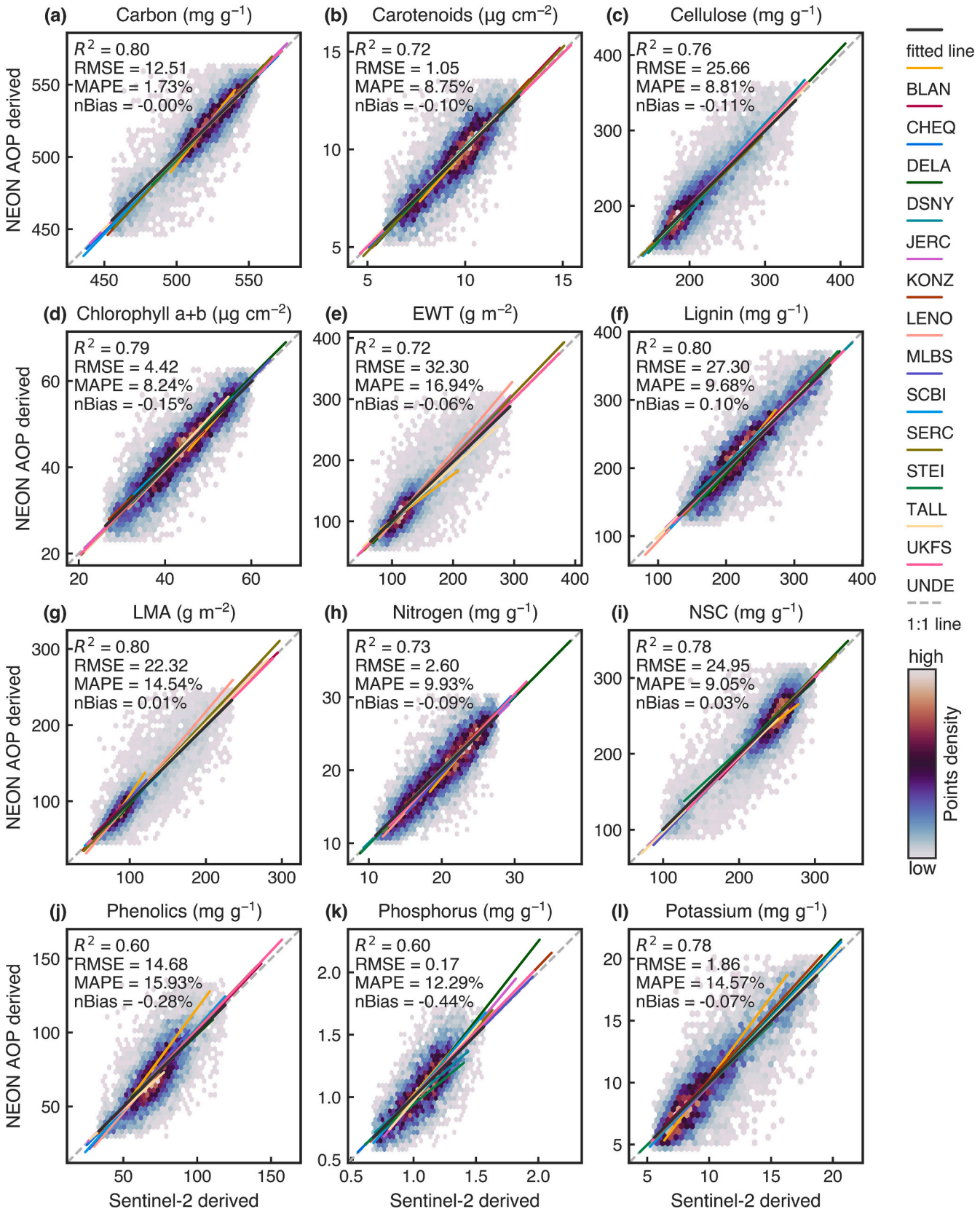

Fig. 4. Overall evaluation of *Time-series RS* models on independent validation sets for 12 foliar functional traits (a-l). Black lines indicate the fitted lines for all sample of independent validation sets. Colored lines indicate the fitted lines for all samples of each site. EWT, equivalent water thickness. LMA, leaf mass per area. NSC, nonstructural carbohydrate. R^2, the coefficient of determination. RMSE, root mean square error. MAPE, mean absolute percentage error. nBias, normalized bias.

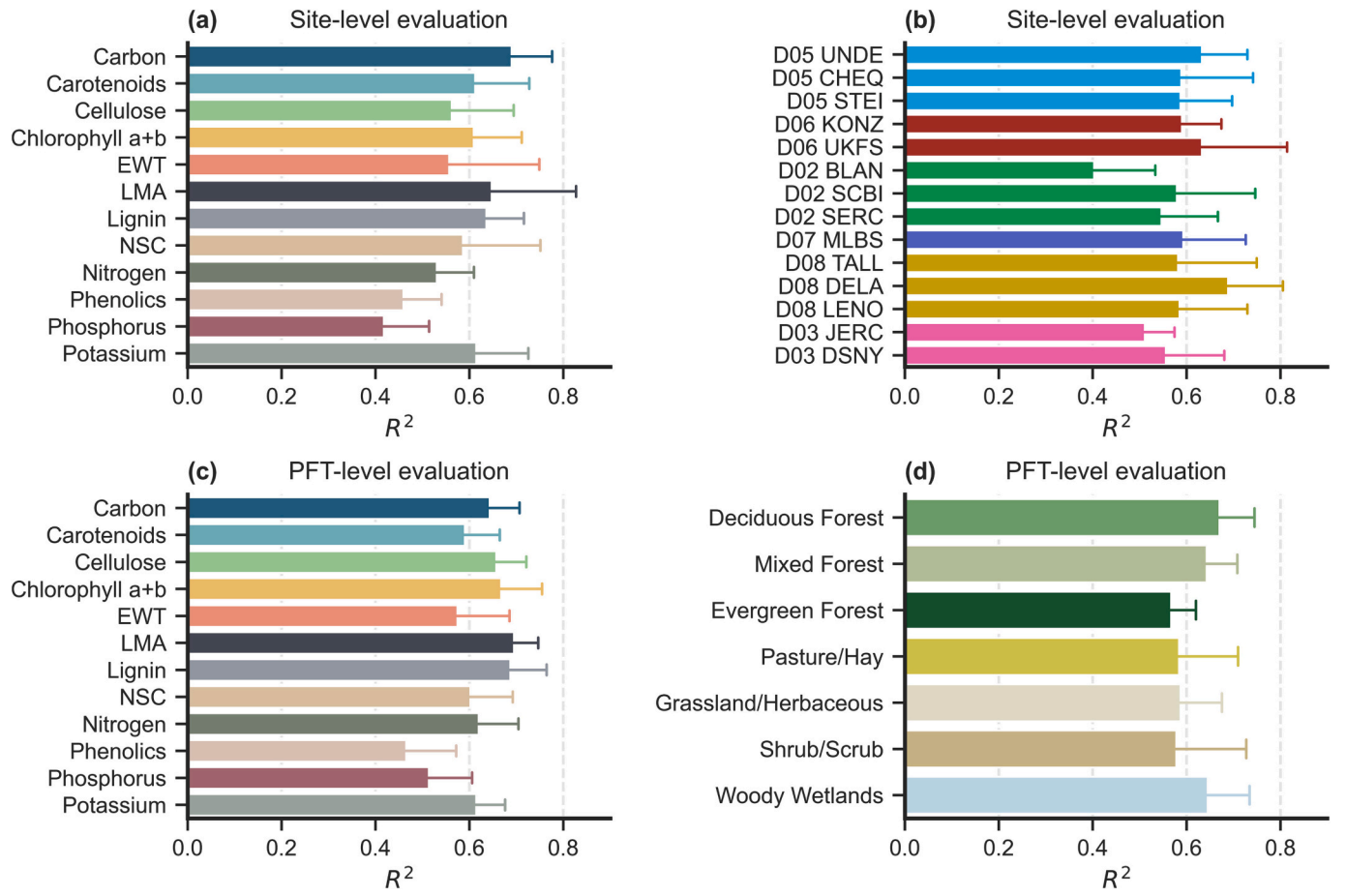

Fig. 5. Site-level evaluation (a, b) and PFT-level evaluation (c, d) of *Time-series RS* models on independent validation sets for 12 foliar functional traits. The length of bars represents the average R^2 across 12 foliar functional traits (a, c) or 14 sites (b) or 7 PFTs (d), while error bar represents the standard deviation. Refer to Table S6. For detailed site-level evaluation results and Table S7. For detailed PFT-level evaluation results.

(Figs. A2 and Fig. A3). For the leave-one-site-out validation, the R^2 for lignin, LMA and NSC was higher than 0.6, whereas phenolics and phosphorus had a R^2 <0.4 (Fig. A2). The remaining seven traits exhibit R^2 values ranging between 0.4 and 0.6 (Fig. A2). Carbon demonstrated the lowest MAPE at 2.72%, while EWT, LMA, phenolics and potassium display higher MAPE between 20 and 25% (Fig. A2). The remaining traits had MAPE between 10 and 20% (Fig. A2). The leave-one-PFT-out validation (Fig. A3) outperformed the leave-one-site-out validation for all 12 traits (Fig. A2), suggesting that *Time-series RS* models can be more successfully transferred to unseen PFTs than to samples that are spatially missing training data. Models trained with other PFTs exhibit relatively accurate predictions (with a moderately low increase in RMSE for the leave-one-PFT-out approach compared to the RMSE of the 80:10:10 split) for deciduous forest, evergreen forest, grassland/herbaceous, and mixed forest. Conversely, the predictions are less accurate for pasture/hay, shrub/scrub, and woody wetlands (Table S9).

3.2. The model performance of foliar traits subject to different input variables

To address Q2, we compared the *Time-series RS* models with four other model scenarios: 1) *Time-series RS* + *Env* models, 2) *Single image RS* models, 3) *Env* models, and 4) *Env* + *PFT* models. Our results revealed that the *Time-series RS* + *Env* models exhibited a marginally higher mean R^2 value of 0.75 compared to *Time-series RS* models with 0.74 (Fig. 6a). The MAPE of *Time-series RS* + *Env* models was, on average, only 0.2% lower than that of *Time-series RS* models (Fig. 6b). We next investigated the utilization of environmental variables alone (*Env* Models) and discovered that the average R^2 value was 0.56, accompanied by an average MAPE value of 14.7% (Fig. 6a and b). Incorporating PFT information into environmental variables (*Env* + *PFT* Models) only marginally improves performance with an average R^2 of 0.59 and MAPE of 14.3% (Fig. 6a and b). This suggests that the *Time-series RS* models can capture within-PFT trait variability, rather than simply learning between-PFT differences. Overall, the absolute nBias for the 5 model scenarios varied but were small on average (<0.5%) (Fig. 6c).

We found that incorporating the phonological variation of remote sensing observation (*Time-series RS* models) significantly improved the predictive power as compared to using a single point in time only (*Single image RS* models), with a significant higher average R^2 value of 0.74 of the *Time-series RS* models compared to 0.53 of the *Single image RS* models (Fig. 6a). Additionally, the average MAPE improved from 15.2% in *Single image RS* models to 10.9% in *Time-series RS* models (Fig. 6b). Regarding specific traits, all traits had R^2 improvement larger than 0.15, with the highest improvement being 0.28 for phosphorus (Fig. 6d). The most significant MAPE improvements were observed for LMA, EWT, and potassium, with MAPE improvements of 8.1%, 6.6% and 6.4%, respectively (Fig. 6e). In contrast, the least improvement was seen for carbon, with a MAPE improvement of only 0.9% (Fig. 6e). Similar results were also observed at the PFT-level evaluation (Fig. A1). We also compared the *Time-series RS* models and *Single image RS* models at PFT-level. Our results revealed that the *Single image RS* model had an average R^2 value of 0.29 at PFT-level (Fig. A1a), compared with average R^2 value of 0.62 of *Time-series RS* models (Fig. A1a). *Time-series RS* models significantly outperformed *Single image RS* models for all traits across all PFTs (Fig. A1b-n).

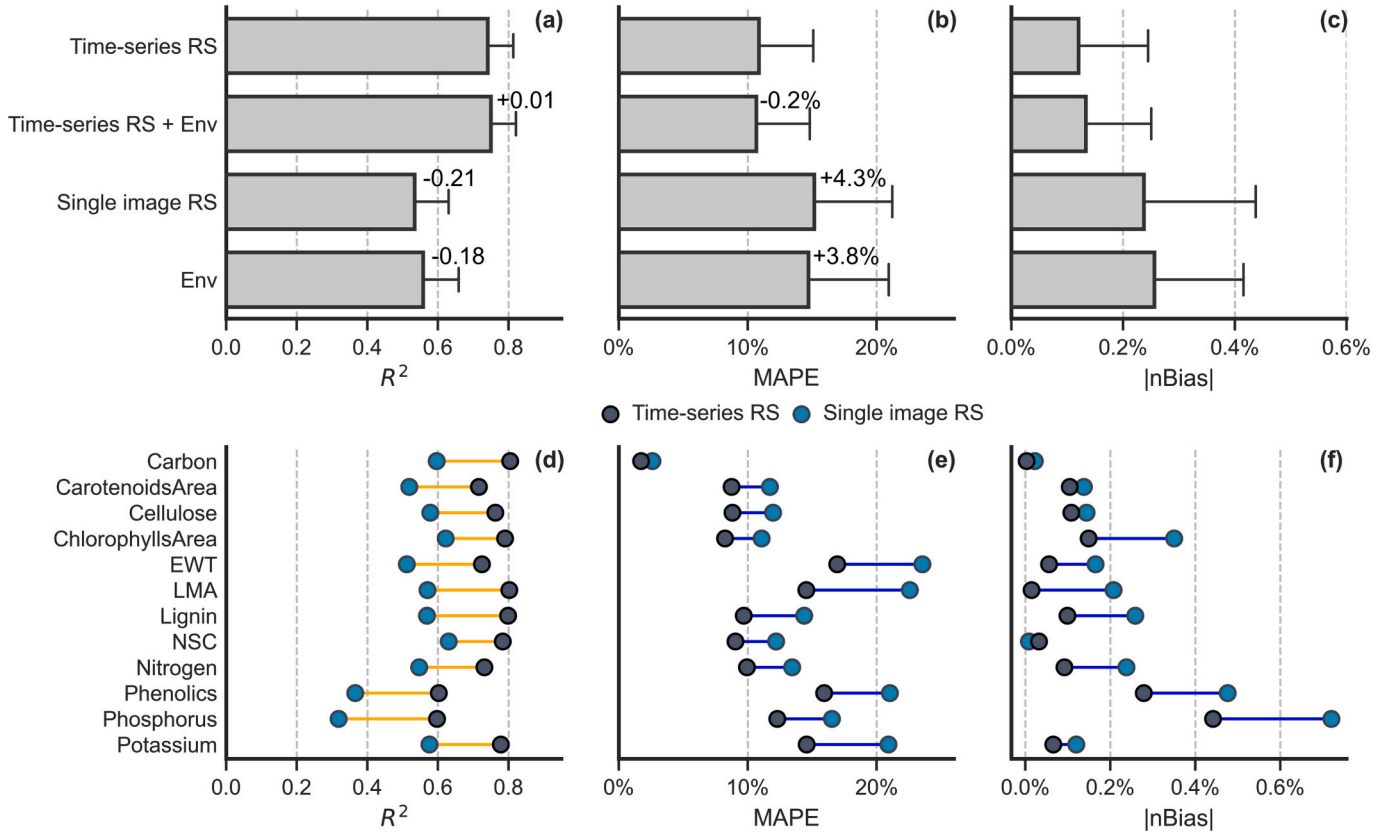

Fig. 6. Comparing *Time-series RS* models, *Time-series RS + Env* models, *Single image RS* models, *Env* and *Env + PFT* Models in terms of R^2 (a), MAPE (b) and absolute nBias (c). The length of bars represents the average R^2 or MAPE or absolute nBias change on the independent validation set across 12 foliar functional trait models, while error bar represents the standard deviation (a-c). (d-f) R^2 (d), MAPE (e) and absolute nBias (f) of each of 12 foliar functional traits using 2 different feature sets (*Time-series RS* and *Single image RS*). R^2, the coefficient of determination. RMSE, root mean square error. MAPE, mean absolute percentage error. nBias, normalized bias.

3.3. Important spectral bands and phenological stages for predicting foliar functional traits

For the Q3, our results demonstrate some clear associations between traits and specific spectral characteristics/phenological stages, but these associations also vary considerably across traits (Fig. 7). Focusing on the association with specific spectral bands, we found blue, green, red, NIR, EVI were identified as important for most of traits, while SWIR2 and MCARI were important for a few traits (Fig. 7).

In addition to the trait-specific association with spectral characteristics, we also observed considerable variations in spectra-trait associations across different growing seasons, with the relative order of season-specific association strength displaying the following four categories (Fig. 7): (I) Autumn > Summer > Spring > Winter; (II) Summer > Spring > Autumn > Winter; (III) Summer > Autumn > Spring > Winter; (IV) Spring = Summer > Autumn > Winter. Specifically, we observed 5 traits (*i.e.*, carbon, carotenoids, NSC, phenolics, potassium) belonging to the category 1 (Fig. 7a, b, i, j, and l), 2 traits (*i.e.*, cellulose, EWT) belonging to the category 2 (Fig. 7c and e), 4 traits (chlorophyll a + b, lignin, nitrogen, phosphorus) belonging to the category 3 (Fig. 7d, f, h, and k), and 1 trait (*i.e.*, LMA) belonging to the category 4 (Fig. 7g).

3.4. Foliar functional maps predicted from time-series Sentinel-2

Fig. 8 shows the trait maps generated using the *Time-series RS* models. We used four traits (LMA, nitrogen, potassium and chlorophyll a + b) for an area of about 5 km^2 at four NEON sites for demonstration (Fig. 8b-e) and compared them with NLCD land cover maps (Fig. 8a). The trait maps illustrated the significant potential of utilizing Sentinel-2 for trait mapping, particularly in characterizing fine spatial details and variations in traits both between and within PFTs. Deciduous forests exhibit lower LMA and higher nitrogen, whereas evergreen forests display higher LMA and lower nitrogen (Fig. 8b and c). In comparison to grasslands, forests generally possess higher potassium and chlorophyll (Fig. 8d and e). KONZ site is predominantly grassland, yet variations in traits still exist within the grassland PFT (Fig. 8).

Predictive uncertainty of the trait maps primarily stems from the lack of training data and secondarily from model prediction errors (Fig. A4). Using LMA maps at three NEON sites as examples, the *Time-series RS* model yielded high prediction uncertainty for water and cultivated crop regions at BLAN (Fig. A4a), water regions at LENO (Fig. A4b), while demonstrated relatively high predictive confidence for most areas at TALL (Fig. A4c). Overall, >75% of the pixels exhibited high predictive confidence (relative uncertainty<0.25) for all traits, except phenolics in the UKFS (Fig. A4d). EWT, LMA, phenolics, and potassium had more pixels with high predictive uncertainty compared to other traits (Fig. A4d), while they also displayed relatively high MAPE during the validation of the *Time-series RS* models (Fig. 4).

We compared trait maps derived from Sentinel-2 with those derived from NEON AOP (Fig. A5). The degree of agreement between the two sets of maps (Fig. A5a-l) was found to be generally consistent with the validation results of the *Time-series RS* model (Fig. 4). This finding indicates that our random point sampling method provides a representative sampling and that the *Time-series RS* model does not overfit the training data. Visual inspection revealed that the model generally reproduced the spatial patterns of NEON AOP trait maps, but underestimated extremely high trait values and overestimated extremely low trait values (Fig. A5m and n).

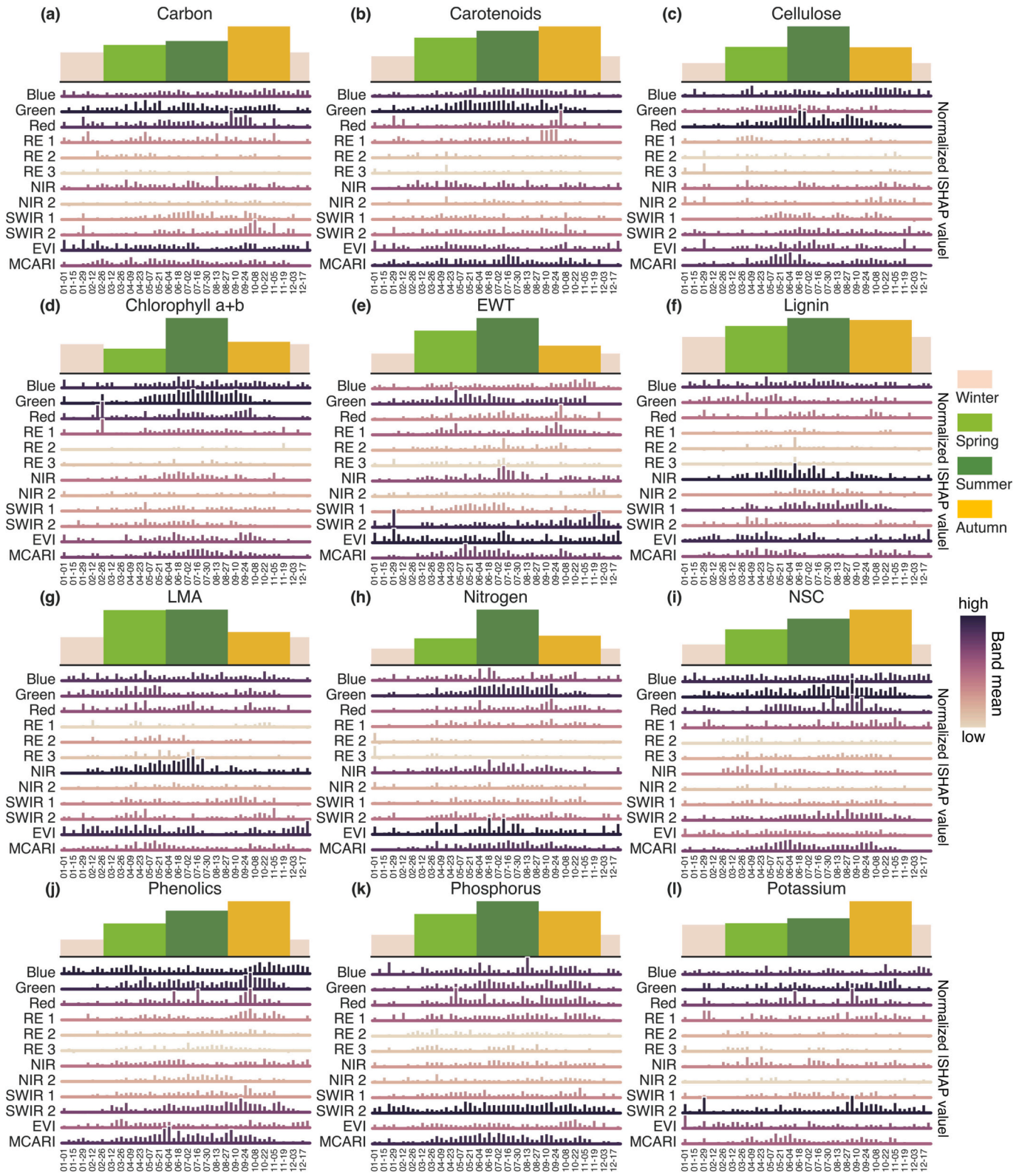

Fig. 7. Analysis of feature importance of *Time-series RS* models using SHAP value across 12 foliar functional traits (a-l). The bars indicate the model-specific-normalized absolute SHAP value (Normalized |SHAP value|). We converted the week number to the first day of each week for clearer demonstration on the x-axis. The bars on top of the subfigure represent the summed normalized |SHAP value| of each season. Spring is defined as weeks 10–22, summer as weeks 23–35, autumn as weeks 36–48, and winter as weeks 1–9 and 50–52. Abbreviations: RE, red-edge; NIR, near-infrared; SWIR, short-wave infrared. (For interpretation of the references to colour in this figure legend, the reader is referred to the web version of this article.)

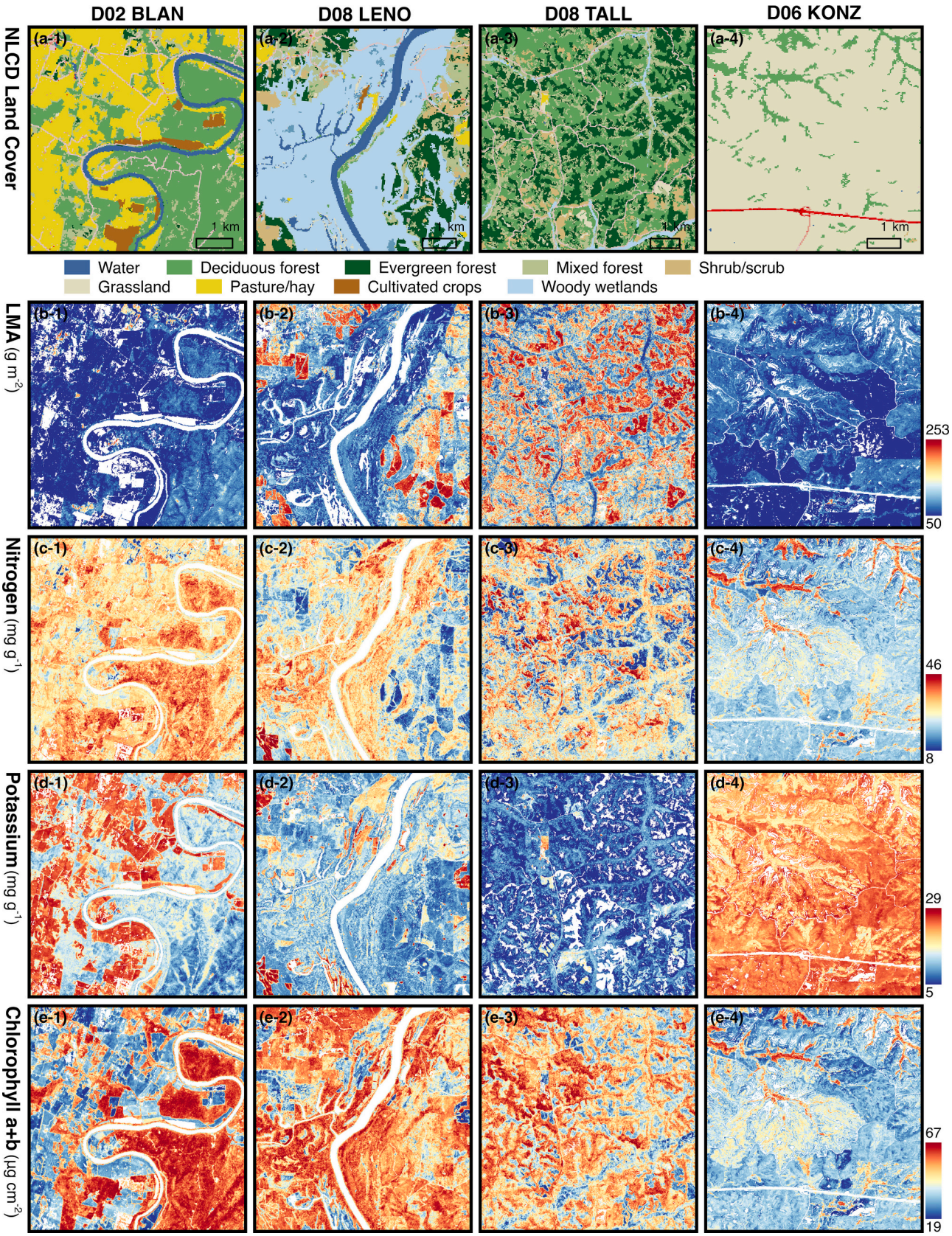

Fig. 8. Land cover (a) and functional trait maps produced by *Time-series RS* models using Sentinel-2 (b-e) at 4 NEON sites. We used 2019 NLCD land cover product (a). We used four traits - LMA (b), nitrogen (c), potassium (d) and chlorophyll a + b (e) - as examples for demonstration.

4. Discussion

4.1. Spectra-phenology integration from multispectral satellite data enables high spatial resolution, large-scale scalability and accurate upscaling of foliar functional traits

In this study, we demonstrated that spectra-phenology integration of Sentinel-2 time-series data can be an accurate approach to mapping multiple foliar traits (Fig. 4, Fig. 8) at a high spatial resolution, capturing intra-site and intra-PFT trait variation (Fig. 5) and offering scalability due to large-scale coverage. The spectra-phenology integration approach is grounded in the physical principles of plant spectroscopy and the ecological trait-phenology association (directly or through species linkages), addressing the limitations of existing trait upscaling strategies. Global-scale studies typically rely on PFT-based and environmental variable-driven statistical method (reviewed by Dechant et al., 2023) or coarse resolution multispectral images (Moreno-Martínez et al., 2018). In contrast, our approach outperforms environmental modeling methods (*Env* models, Fig. 6) in our 14 NEON sites with a wide range of environmental gradients, although our approach is not validated on a global scale. Furthermore, we observed considerable variability within each PFT for all 12 traits (Fig. 3), and the *Time-series RS* models captured this variability well (Fig. 5), making it logically obvious that our method is superior to methods based only on PFT lookup tables which ignores the trait variation within a PFT. The importance of within-PFT trait has prompted numerous prior research endeavors to incorporate environmental variables, spatial models, or remote sensing temporal and spectral metrics, in addition to solely utilizing PFT information (Dechant et al., 2023).

Compared to previous studies on regional-scale multi-trait mapping (Aguirre-Gutiérrez et al., 2021; Asner et al., 2017; Wallis et al., 2019), our study demonstrates the following advantages. We upscaled from *in-situ* trait observations to landscape-scale and then regional-scale, following the strategy in Asner et al. (2017), however, our approach can provide trait maps with higher resolution (10 m *vs.* 1 km) and prediction accuracy (compared to the *Env* models, Fig. 6). The *Time-series RS* models also outperforms the *Single image RS* models used in Aguirre-Gutiérrez et al. (2021) and Wallis et al. (2019) and greatly improves the PFT-level evaluation (Figs. 5 and A1). More importantly, the proposed approach overcomes the coverage limitation of airborne imaging spectroscopy (Wessman et al., 1988; Martin et al., 2008; Asner et al., 2015; Wang et al., 2020) and offers significantly enhanced scalability by utilizing Sentinel-2 data with global coverage. Note that we have only compared the *Time-series RS* model with the primary methods and variables used in existing studies. While these methods were also used in combination (*e.g. Single image RS* + *Env* in Aguirre-Gutiérrez et al., 2021), and the utilization of various satellite data sources have been explored (*e.g.* MODIS data used in Moreno-Martínez et al., 2018), we have not exhausted all possible combinations in our comparison (Fig. 6).

Our spectra-phenology integration approach can effectively capture trait variation without using environmental variables (*Time-series RS* models *vs. Time-series RS* + *Env* models, Fig. 6). The lack of necessity for environmental variables is also supported by a plant species classification study using dense time-series Sentinel-2 images (Hemmerling et al., 2021). One possible explanation is a strong correlation between plant phenology and macro-climate. Given that phenological information was implicitly incorporated into the *Time-series RS* model, environmental factors did not contribute too much additional information. In contrast, incorporating environmental variables in models lacking time series data enhances model accuracy (Aguirre-Gutiérrez et al., 2021; Loozen et al., 2020; Wallis et al., 2019). Another potential reason is that traits are actually influenced by micro-environmental factors (Gagliardi et al., 2021; López et al., 2016; Sanczuk et al., 2023), while most of the environmental variable data used in our study is only capable to characterize macro-environmental variation. We chose to use *Time-series RS* models without macro-environmental variables for the final mapping products, because compared with *Time-series RS* models, *Time-series RS* + *Env* models did not increased accuracy in terms of both R^2 and MAPE (Fig. A6a and b), but rather, they increased the bias (Fig. A6c) when extrapolated to unseen sites. This can also potentially present opportunities for understanding the environmental regulation of traits at larger scales. Moreover, our study found that exclusion of canopy texture variables from *Time-series RS* models did not reduce the predictive power (Fig. S4). This may be because the biophysical information represented by texture variables are not clear at a 10 m spatial resolution (Hemmerling et al., 2021), unlike spectra-phenology features that are generalized across species, life forms, and regions (Serbin et al., 2019; Wright et al., 2004).

4.2. Biophysical and ecological mechanism of time-series RS models

The *Time-series RS* models successfully upscale traits due to both spectral and phenological factors. Our analysis of the feature importance of *Time-series RS* models in summer generally aligned with previous literature findings regarding crucial spectral region for canopy-level trait prediction. Bands in visible wavelengths are more important for predicting pigments (carotenoids, chlorophyll a + b, Fig. A7, Martin et al., 2018, Ustin et al., 2009) and traits associated with pigments (nitrogen, phosphorus, Fig. A7, Martin et al., 2018). The NIR band is predominantly important for predicting LMA and EWT (Fig. A7) which is supported by Asner et al. (2011). The NIR band is also important for carbon and lignin (Fig. A7), which normally co-vary with LMA (Martin et al., 2018). SWIR bands proves important for predicting phenolics, phosphorus, and potassium (Fig. A7), as phenolics has absorption features in the SWIR region (Curran, 1989; Fourty et al., 1996; Kokaly and Skidmore, 2015), and previous literature has emphasized their importance for predicting phosphorus and potassium (Chadwick and Asner, 2016). The only unexpected result is the modeling for cellulose, where the red band is most important, while the SWIR bands are not (Fig. A7). This is potentially because the Sentinel-2 SWIR 1 band (1610 nm with 90 nm band width, Table 1) does not cover the strong absorption feature of cellulose (1780 nm, Curran, 1989), making the model-predicted cellulose a consequence of the covariation with other traits.

Our results indicate that while summer spectral features are generally more important, they do not greatly surpass the importance of other seasons (Fig. 7), highlighting the relevance of phenology information in trait prediction. Previous studies have also recognized the value of non-summer spectral features, such as utilizing time-series remote sensing for plant species classification (Cai et al., 2018; Grabska et al., 2020; Hemmerling et al., 2021), grassland land-use intensity assessment (Lange, 2022), and crop yield estimation (Hunt et al., 2019). In addition to analyzing feature importance, we further investigated whether a widely recognized theory of phenology-foliar trait coordination, the leaf economics spectrum (LES) (Reich et al., 1997; Wright et al., 2004), remains valid in our data.

In LES theory, leaf longevity co-varies with other foliar traits along a 'fast-slow' principal axis (Reich et al., 1997; Wright et al., 2004). Following the assumption of Running et al. (1995), we used the vegetation index (VI) amplitude as a remote sensing proxy for leaf longevity and employed the two band Enhanced Vegetation Index (EVI2) derived from multi-sensor land surface phenology (MS-LSP) product (Bolton et al., 2020) (see detail in Method S1). Plants with longer leaf longevity tend to exhibit lower VI amplitude, and *vice versa* (Running et al., 1995). We found that a single principal axis (PC 1) accounted for 74% of the covariation among EVI2 amplitude, LMA, and nitrogen across different PFTs (Fig. 9). Fast-return plants exhibit high leaf nitrogen, high EVI2 amplitude, and low LMA (Fig. 9). In contrast, plants with higher EVI2 amplitude, high LMA, and low leaf nitrogen demonstrate slower returns (Fig. 9). Within each PFT, the principal axis can still explain a substantial amount of covariation (50.8%–73.7%, Fig. A8), suggesting the coordination is maintained across major PFTs. Similarly, Moreno-Martínez

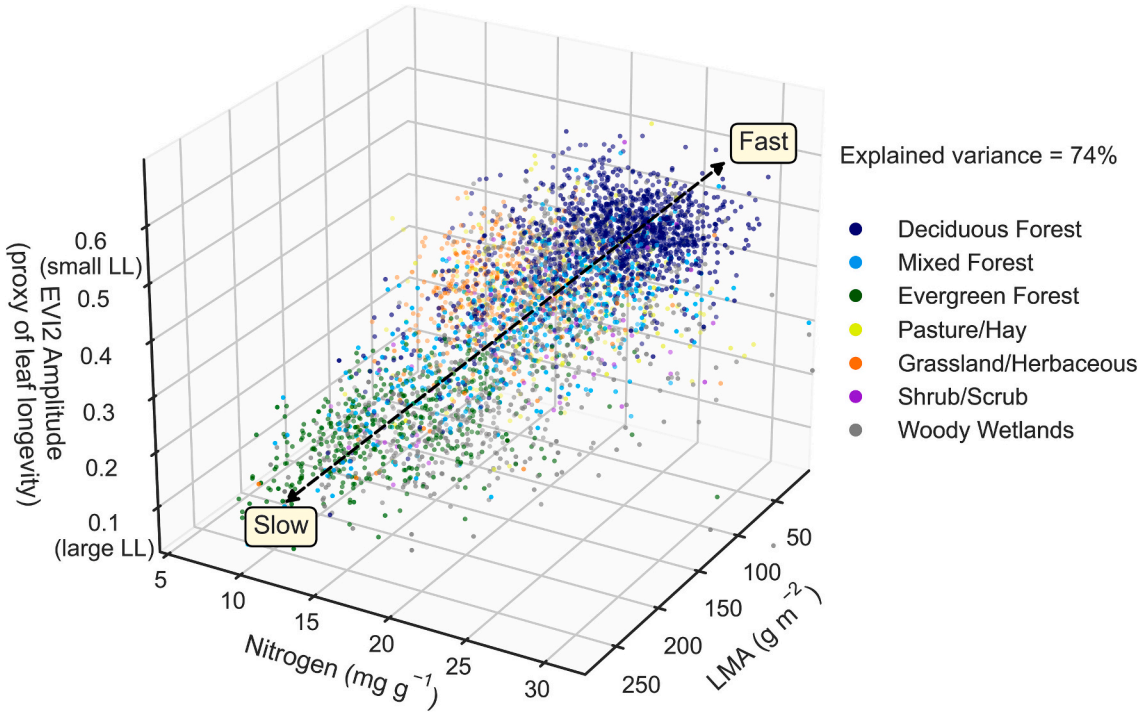

Fig. 9. The covariation of LMA, nitrogen and EVI2 amplitude (remote-sensing proxy of leaf longevity) in a 'fast-slow' axis in three-dimensional space. The black dashed line indicates the direction of the first principal component. The point colors represent the PFT. LL, leaf longevity.

et al. (2018) found that VI max and VI std. were crucial for multi-trait prediction, with both metrics strongly correlating with VI amplitude. Our revalidation of LES reveals a direct correlation between plant traits and phenological characteristics, such as EVI2 amplitude. The *Time-series RS* models already contain information on EVI2 amplitude (Fig. S5), as the EVI2 amplitude is the difference between minimum and maximum greenness over a year and the inclusion of it did not increase model accuracy (results not shown). Thereby, the *Time-series RS* models could potentially use the information of EVI2 amplitude for trait prediction. Moreover, the *Time-series RS* models may predict traits based on trait-trait coordination or relationships between traits and other phenological characteristics. For example, literature found a link between leaf senescence date and carbon content (Bucher and Römermann, 2021; Sporbert et al., 2022), but more in-depth analyses are needed.

Another potential mechanism of the *Time-series RS* models involves leveraging the differences in phenological rhythms among plant species. Differences in plant phenology (seasonal changes in greenness) among species have been reported (Chuine and Beaubien, 2001; Richardson, 2019). Concurrently, past researches have used temporal information from satellite to estimate traits (Moreno-Martínez et al., 2018), and have demonstrated that employing satellite time-series spectral data enhances plant species discrimination compared to relying on single-time plant reflectance spectra (Grabska et al., 2020; Hemmerling et al., 2021). Given the interspecific trait variations (Díaz et al., 2016; Wang et al., 2022; Wright et al., 2004), the *Time-series RS* models can predict traits by differentiating between species. In this context, there is no causal relationship between foliar traits and phenology; rather, both are characteristics of the plant species. Importantly, the *Time-series RS* models can improve species identification, thereby increasing the accuracy of trait predictions.

4.3. Limitations

In this study, we utilized time-series Sentinel-2 data to obtain phenology information for modeling traits. However, cloud contamination of satellite data reduces the availability of time-series observations, particularly in regions with frequent cloud cover. To address this issue, we employed a four-year composite approach to generate dense time-series image collections. Nevertheless, this multi-year compositing approach is unsuitable for vegetated areas where phenological characteristics exhibit considerable inter-annual variations, such as croplands, vegetation subject to disturbance or logging, or rapidly growing young forests. Also, our benchmarks were trait maps derived from airborne imaging spectroscopy rather than *in-situ* trait observations. We opted for trait maps as benchmarks due to two benefits: increased sample size and range for model training, and reduction of error in matching satellite imagery and *in-situ* data. However, since the trait maps are generated using PLSR models, their representativeness of real-world trait variation may be less accurate compared to *in-situ* data. *In-situ* data also have limitations, as scaling traits for a limited number of leaf measurements to the satellite image pixel remains challenging (Dechant et al., 2023). Finally, the method was tested across a limited set of sites and geographical regions, and its transferability needs to be assessed in new areas with potentially differing phenology and spectral characteristics. Also, because the training data are not representative of the global variability of traits, the model can only be confidently upscaled to the regional scale.

4.4. Implications

The results of this research provide opportunities to address current real-world challenges and to tackle ongoing and future ecological questions. NEON domains are designed to be representative of the ecosystems of the United States; as such, our models can be applied across the eastern United States to develop spatially continuous maps that include tens of foliar traits. For instance, these maps could be used to examine broad patterns of trait-trait coordination (Asner et al., 2016), trait-environment relationships (Joswig et al., 2022; Wang et al., 2022), and the processes underlying whether and how functional diversity regulates ecosystem productivity (Durán et al., 2019; Gomarasca et al., 2023; Schneider et al., 2017). Trait maps can enhance the representative

of ecosystem processes by more accurately characterizing vegetation (Schneider et al., 2023; Wieczynski et al., 2022) in Earth system models, serving as a foundation for predicting responses to environmental change. In addition, these trait maps may provide baseline data to identify biodiversity hotspots, thus contributing to the development of local biodiversity conservation policies (Cavender-Bares et al., 2022). As the integration of phenology information is inspired by the coordination and trade-offs in plant traits, this approach may hold potential not only for inference of foliar traits, but also for other traits, *e.g.*, related to plant canopy structure and belowground processes (Cavender-Bares et al., 2021; Díaz et al., 2016).

Our study presents opportunities to use archived satellite observations to infer coarse-scale changes in plant traits. Satellite observations have long been used to classify the world into various vegetation types (Defries and Townshend, 1994; Running et al., 1995), such as forests and grasslands, or more specifically, leaf area index or forest cover (Hansen et al., 2013; Myneni et al., 2002), contributing to Earth system studies. Using models such as those presented in this paper, the long time-series satellite observations from Landsat could be used to implement the spectra-phenology integration approach in conjunction with historical *in-situ* trait observations. This potentially enables the development of spatially and temporally universal trait prediction models and provides an essential way forward for future global trait mapping. As well, this may provide additional documentation to support the identification of biodiversity loss (Cavender-Bares et al., 2022; Jetz et al., 2016; Skidmore et al., 2021).

5. Conclusion

In this study, we investigated a spectra-phenology integration approach for modeling and mapping 12 foliar functional traits using time-series Sentinel-2 data in the eastern United States. We demonstrated that combining time-series Sentinel-2 data with machine learning regression can effectively capture the variation of all 12 traits for overall, site-level, and PFT-level evaluation (Figs. 4 and 5). The spectra-phenology integration approach outperformed existing methods (which rely on environmental proxies or a single satellite image as predictors) without necessarily requiring additional environmental variables as input (Fig. 6). Both the biophysical and ecological mechanisms of the proposed method are consistent with established literature and LES theory (Figs. 7 and 9). Collectively, we demonstrated that spectra-phenology integration using time-series Sentinel-2 data can serve as an accurate, high-throughput, and scalable method for high spatial-resolution mapping of foliar traits, opening new avenues for mapping and monitoring foliar functional traits at regional and global scales. This study offers a valuable contribution to the field of remote sensing and functional ecology, with the potential to advance our understanding of plant traits and their role in ecosystem processes.

CRediT authorship contribution statement

Shuwen Liu: Conceptualization, Formal analysis, Investigation, Methodology, Visualization, Writing – original draft. **Zhihui Wang:** Resources, Supervision, Writing – review & editing. **Ziyu Lin:** Methodology. **Yingyi Zhao:** Writing – review & editing. **Marco Visser:** Writing – review & editing. **Philip A. Townsend:** Resources, Writing – review & editing. **Jin Wu:** Conceptualization, Funding acquisition, Investigation, Supervision, Visualization, Writing – review & editing. **Kun Zhang:** Writing – review & editing. **Zhengbing Yan:** Writing – review & editing.

Declaration of Competing Interest

The authors declare that they have no known competing financial interests or personal relationships that could have appeared to influence the work reported in this paper.

Data availability

Data will be made available on request.

Acknowledgments

This work was supported by the National Natural Science Foundation of China(#31922090), Hong Kong Research Grant Council General Research Fund (#17305321), and the HKU Seed Funding for Strategic Interdisciplinary Research Scheme. J.Wu was also in part supported by Hong Kong Research Grant Council Collaborative Research Fund (#C5062-21GF), the Hung Ying Physical Science Research Fund 2021-22, and the Innovation and Technology Fund (funding support to State Key Laboratories in Hong Kong of Agrobiotechnology) of the HKSAR, China. Z.W. was supported by GDAS' Special Project of Science and Technology Development (2020GDASYL-20200102001). P.A.T. was supported by the US National Science Foundation (NSF), Macrosystems Biology and NEON-Enabled Science grant DEB-1638720 and NSF Biology Integration Institute award ASCEND, DBI-2021898.

Appendix A. Supplementary data

Supplementary data to this article can be found online at https://doi.org/10.1016/j.rse.2024.114082.

References

Aguirre-Gutiérrez, J., Rifai, S., Shenkin, A., Oliveras, I., Bentley, L.P., Svátek, M., Girardin, C.A.J., Both, S., Riutta, T., Berenguer, E., Kissling, W.D., Bauman, D., Raab, N., Moore, S., Farfan-Rios, W., Figueiredo, A.E.S., Reis, S.M., Ndong, J.E., Ondo, F.E., N'ssi Bengone, N., Mihindou, V., Moraes De Seixas, M.M., Adu-Bredu, S., Abernethy, K., Asner, G.P., Barlow, J., Burslem, D.F.R.P., Coomes, D.A., Cernusak, L. A., Dargie, G.C., Enquist, B.J., Ewers, R.M., Ferreira, J., Jeffery, K.J., Joly, C.A., Lewis, S.L., Marimon-Junior, B.H., Martin, R.E., Morandi, P.S., Phillips, O.L., Quesada, C.A., Salinas, N., Schwantes Marimon, B., Silman, M., Teh, Y.A., White, L.J. T., Malhi, Y., 2021. Pantropical modelling of canopy functional traits using Sentinel-2 remote sensing data. Remote Sens. Environ. 252, 112122. https://doi.org/10.1016/j.rse.2020.112122.

Akiba, T., Sano, S., Yanase, T., Ohta, T., Koyama, M., 2019. Optuna: a next-generation hyperparameter optimization framework. In: Proceedings of the 25th ACM SIGKDD International Conference on Knowledge Discovery & Data Mining, KDD '19. Association for Computing Machinery, New York, NY, USA, pp. 2623–2631. https://doi.org/10.1145/3292500.3330701.

Asner, G.P., Martin, R.E., Tupayachi, R., Emerson, R., Martinez, P., Sinca, F., Powell, G. V., Wright, S.J., Lugo, A.E., 2011. Taxonomy and remote sensing of leaf mass per area (LMA) in humid tropical forests. Ecol. Appl. 21, 85–98.

Asner, G.P., Knapp, D.E., Boardman, J., Green, R.O., Kennedy-Bowdoin, T., Eastwood, M., Martin, R.E., Anderson, C., Field, C.B., 2012. Carnegie airborne Observatory-2: increasing science data dimensionality via high-fidelity multi-sensor fusion. Remote Sens. Environ. 124, 454–465. https://doi.org/10.1016/j.rse.2012.06.012.

Asner, G.P., Martin, R.E., Anderson, C.B., Knapp, D.E., 2015. Quantifying forest canopy traits: imaging spectroscopy versus field survey. Remote Sens. Environ. 158, 15–27. https://doi.org/10.1016/j.rse.2014.11.011.

Asner, G.P., Knapp, D.E., Anderson, C.B., Martin, R.E., Vaughn, N., 2016. Large-scale climatic and geophysical controls on the leaf economics spectrum. Proc. Natl. Acad. Sci. U. S. A. 113, E4043–E4051. https://doi.org/10.1073/pnas.1604863113.

Asner, G.P., Martin, R.E., Knapp, D.E., Tupayachi, R., Anderson, C.B., Sinca, F., Vaughn, N.R., Llactayo, W., 2017. Airborne laser-guided imaging spectroscopy to map forest trait diversity and guide conservation. Science 355, 385–389. https://doi.org/10.1126/science.aaj1987.

Bjorkman, A.D., Myers-Smith, I.H., Elmendorf, S.C., Normand, S., Rüger, N., Beck, P.S.A., Blach-Overgaard, A., Blok, D., Cornelissen, J.H.C., Forbes, B.C., Georges, D., Goetz, S.J., Guay, K.C., Henry, G.H.R., HilleRisLambers, J., Hollister, R.D., Karger, D. N., Kattge, J., Manning, P., Prevéy, J.S., Rixen, C., Schaepman-Strub, G., Thomas, H. J.D., Vellend, M., Wilmking, M., Wipf, S., Carbognani, M., Hermanutz, L., Lévesque, E., Molau, U., Petraglia, A., Soudzilovskaia, N.A., Spasojevic, M.J., Tomaselli, M., Vowles, T., Alatalo, J.M., Alexander, H.D., Anadon-Rosell, A., Angers-Blondin, S., te Beest, M., Berner, L., Björk, R.G., Buchwal, A., Buras, A., Christie, K., Cooper, E.J., Dullinger, S., Elberling, B., Eskelinen, A., Frei, E.R., Grau, O., Grogan, P., Hallinger, M., Harper, K.A., Heijmans, M.M.P.D., Hudson, J., Hülber, K., Iturrate-Garcia, M., Iversen, C.M., Jaroszynska, F., Johnstone, J.F., Jørgensen, R.H., Kaarlejärvi, E., Klady, R., Kuleza, S., Kulonen, A., Lamarque, L.J., Lantz, T., Little, C. J., Speed, J.D.M., Michelsen, A., Milbau, A., Nabe-Nielsen, J., Nielsen, S.S., Ninot, J. M., Oberbauer, S.F., Olofsson, J., Onipchenko, V.G., Rumpf, S.B., Semenchuk, P., Shetti, R., Collier, L.S., Street, L.E., Suding, K.N., Tape, K.D., Trant, A., Treier, U.A., Tremblay, J.P., Tremblay, M., Venn, S., Weijers, S., Zamin, T., Boulanger-Lapointe, N., Gould, W.A., Hik, D.S., Hofgaard, A., Jónsdóttir, I.S., Jorgenson, J.,

Klein, J., Magnusson, B., Tweedie, C., Wookey, P.A., Bahn, M., Blonder, B., van Bodegom, P.M., Bond-Lamberty, B., Campetella, G., Cerabolini, B.E.L., Chapin, F.S., Cornwell, W.K., Craine, J., Dainese, M., de Vries, F.T., Díaz, S., Enquist, B.J., Green, W., Milla, R., Niinemets, Ü., Onoda, Y., Ordoñez, J.C., Ozinga, W.A., Penuelas, J., Poorter, H., Poschlod, P., Reich, P.B., Sandel, B., Schamp, B., Sheremetev, S., Weiher, E., 2018. Plant functional trait change across a warming tundra biome. Nature 562, 57–62. https://doi.org/10.1038/s41586-018-0563-7.

Blumenthal, D.M., Mueller, K.E., Kray, J.A., Ocheltree, T.W., Augustine, D.J., Wilcox, K. R., 2020. Traits link drought resistance with herbivore defence and plant economics in semi-arid grasslands: the central roles of phenology and leaf dry matter content. J. Ecol. 108, 2336–2351. https://doi.org/10.1111/1365-2745.13454.

Bolton, D.K., Gray, J.M., Melaas, E.K., Moon, M., Eklundh, L., Friedl, M.A., 2020. Continental-scale land surface phenology from harmonized Landsat 8 and Sentinel-2 imagery. Remote Sens. Environ. 240, 111685. https://doi.org/10.1016/j.rse.2020.111685.

Boonman, C.C.F., Benítez-López, A., Schipper, A.M., Thuiller, W., Anand, M., Cerabolini, B.E.L., Cornelissen, J.H.C., Gonzalez-Melo, A., Hattingh, W.N., Higuchi, P., Laughlin, D.C., Onipchenko, V.G., Peñuelas, J., Poorter, L., Soudzilovskaia, N.A., Huijbregts, M.A.J., Santini, L., 2020. Assessing the reliability of predicted plant trait distributions at the global scale. Glob. Ecol. Biogeogr. 29, 1034–1051. https://doi.org/10.1111/geb.13086.

Bucher, S.F., Römermann, C., 2021. The timing of leaf senescence relates to flowering phenology and functional traits in 17 herbaceous species along elevational gradients. J. Ecol. 109, 1537–1548. https://doi.org/10.1111/1365-2745.13577.

Butler, E.E., Datta, A., Flores-Moreno, H., Chen, M., Wythers, K.R., Fazayeli, F., Banerjee, A., Atkin, O.K., Kattge, J., Amiaud, B., Blonder, B., Boenisch, G., Bond-Lamberty, B., Brown, K.A., Byun, C., Campetella, G., Cerabolini, B.E.L., Cornelissen, J.H.C., Craine, J.M., Craven, D., De Vries, F.T., Díaz, S., Domingues, T. F., Forey, E., González-Melo, A., Gross, N., Han, W., Hattingh, W.N., Hickler, T., Jansen, S., Kramer, K., Kraft, N.J.B., Kurokawa, H., Laughlin, D.C., Meir, P., Minden, V., Niinemets, Ü., Onoda, Y., Peñuelas, J., Read, Q., Sack, L., Schamp, B., Soudzilovskaia, N.A., Spasojevic, M.J., Sosinski, E., Thornton, P.E., Valladares, F., Van Bodegom, P.M., Williams, M., Wirth, C., Reich, P.B., Schlesinger, W.H., 2017. Mapping local and global variability in plant trait distributions. Proc. Natl. Acad. Sci. U. S. A. 114, E10937–E10946. https://doi.org/10.1073/pnas.1708984114.

Cai, Y., Guan, K., Peng, J., Wang, S., Seifert, C., Wardlow, B., Li, Z., 2018. A high-performance and in-season classification system of field-level crop types using time-series Landsat data and a machine learning approach. Remote Sens. Environ. 210, 35–47. https://doi.org/10.1016/j.rse.2018.02.045.

Cavender-Bares, J.M., Schweiger, A.K., Gamon, J.A., Gholizadeh, H., Helzer, K., Lapadat, C., Madritch, M.D., Townsend, P.A., Wang, Z., Hobbie, S.E., 2021. Remotely detected aboveground plant function predicts belowground processes in two prairie diversity experiments. Ecological monographs 0, 1–23. https://doi.org/10.1002/ecm.1488.

Cavender-Bares, J., Schneider, F.D., Santos, M.J., Armstrong, A., Carnaval, A., Dahlin, K. M., Fatoyinbo, L., Hurtt, G.C., Schimel, D., Townsend, P.A., Ustin, S.L., Wang, Z., Wilson, A.M., 2022. Integrating remote sensing with ecology and evolution to advance biodiversity conservation. Nat. Ecol. Evol. https://doi.org/10.1038/s41559-022-01702-5.

Chacón-Labella, J., Hinojo-Hinojo, C., Bohner, T., Castorena, M., Violle, C., Vandvik, V., Enquist, B.J., 2022. How to improve scaling from traits to ecosystem processes. Trends Ecol. Evol. https://doi.org/10.1016/j.tree.2022.10.007.

Chadwick, K., Asner, G., 2016. Organismic-scale remote sensing of canopy foliar traits in lowland tropical forests. Remote Sens. (Basel) 8, 87. https://doi.org/10.3390/rs8020087.

Chen, T., Guestrin, C., 2016. XGBoost: a scalable tree boosting system. In: Proceedings of the 22nd ACM SIGKDD International Conference on Knowledge Discovery and Data Mining, pp. 785–794. https://doi.org/10.1145/2939672.2939785.

Chuine, I., Beaubien, E.G., 2001. Phenology is a major determinant of tree species range. Ecol. Lett. 4, 500–510. https://doi.org/10.1046/j.1461-0248.2001.00261.x.

Claverie, M., Ju, J., Masek, J.G., Dungan, J.L., Vermote, E.F., Roger, J.-C., Skakun, S.V., Justice, C., 2018. The harmonized Landsat and Sentinel-2 surface reflectance data set. Remote Sens. Environ. 219, 145–161. https://doi.org/10.1016/j.rse.2018.09.002.

Curran, P.J., 1989. Remote sensing of foliar chemistry. Remote Sens. Environ. 30, 271–278. https://doi.org/10.1016/0034-4257(89)90069-2.

Daughtry, C.S.T., Walthall, C.L., Kim, M.S., De Colstoun, E.B., McMurtrey, J.E., 2000. Estimating corn leaf chlorophyll concentration from leaf and canopy reflectance. Remote Sens. Environ. 74, 229–239. https://doi.org/10.1016/S0034-4257(00)00113-9.

Dechant, B., Kattge, J., Pavlick, R., Schneider, F., Sabatini, F., Moreno-Martinez, A., Butler, E., Van Bodegom, P., Vallicrosa, H., Kattenborn, T., Boonman, C., Madani, N., Wright, I., Dong, N., Feilhauer, H., Penuelas, J., Sardans, J., Aguirre-Gutierrez, J., Reich, P., Leitao, P., Cavender-Bares, J., Myers-Smith, I., Duran, S., Croft, H., Prentice, I., Huth, A., Rebel, K., Zaehle, S., Simova, I., Diaz, S., Reichstein, M., Schiller, C., Bruehlheide, H., Mahecha, M., Wirth, C., Malhi, Y., Townsend, P., 2023. Intercomparison of global foliar trait maps reveals fundamental differences and limitations of upscaling approaches (preprint). Life Sci. https://doi.org/10.31223/X58S97.

Defries, R.S., Townshend, J.R.G., 1994. NDVI-derived land cover classifications at a global scale. Int. J. Remote Sens. 15, 3567–3586. https://doi.org/10.1080/01431169408954345.

Dewitz, J., 2021. National Land Cover Database (NLCD) 2019 Products. https://doi.org/10.5066/P9KZCM54.

Díaz, S., Kattge, J., Cornelissen, J.H.C., Wright, I.J., Lavorel, S., Dray, S., Reu, B., Kleyer, M., Wirth, C., Colin Prentice, I., Garnier, E., Bönisch, G., Westoby, M., Poorter, H., Reich, P.B., Moles, A.T., Dickie, J., Gillison, A.N., Zanne, A.E., Chave, J., Joseph Wright, S., Sheremet Ev, S.N., Jactel, H., Baraloto, C., Cerabolini, B., Pierce, S., Shipley, B., Kirkup, D., Casanoves, F., Joswig, J.S., Günther, A., Falczuk, V., Rüger, N., Mahecha, M.D., Gorné, L.D., 2016. The global spectrum of plant form and function. Nature 529, 167–171. https://doi.org/10.1038/nature16489.

Durán, S.M., Martin, R.E., Díaz, S., Maitner, B.S., Malhi, Y., Salinas, N., Shenkin, A., Silman, M.R., Wieczynski, D.J., Asner, G.P., Bentley, L.P., Savage, V.M., Enquist, B. J., 2019. Informing trait-based ecology by assessing remotely sensed functional diversity across a broad tropical temperature gradient. Sci. Adv. 5, 1–12. https://doi.org/10.1126/sciadv.aaw8114.

Elvidge, C.D., 1990. Visible and near infrared reflectance characteristics of dry plant materials. Int. J. Remote Sens. 11, 1775–1795. https://doi.org/10.1080/01431169008955129.

Féret, J.-B., Berger, K., de Boissieu, F., Malenovský, Z., 2021. PROSPECT-PRO for estimating content of nitrogen-containing leaf proteins and other carbon-based constituents. Remote Sens. Environ. 252, 112173. https://doi.org/10.1016/j.rse.2020.112173.

Field, C., 1991. Ecological scaling of carbon gain to stress and resource availability. Integr. Responses Plants Stress 35–65.

Fourty, Th., Baret, F., Jacquemoud, S., Schmuck, G., Verdebout, J., 1996. Leaf optical properties with explicit description of its biochemical composition: direct and inverse problems. Remote Sens. Environ. 56, 104–117. https://doi.org/10.1016/0034-4257(95)00234-0.

Funk, J.L., Larson, J.E., Ames, G.M., Butterfield, B.J., Cavender-Bares, J., Firn, J., Laughlin, D.C., Sutton-Grier, A.E., Williams, L., Wright, J., 2017. Revisiting the holy grail: using plant functional traits to understand ecological processes. Biol. Rev. 92, 1156–1173. https://doi.org/10.1111/brv.12275.

Furey, G.N., Tilman, D., 2023. Plant chemical traits define functional and phylogenetic axes of plant biodiversity. Ecol. Lett. https://doi.org/10.1111/ele.14262 ele.14262.

Gagliardi, S., Avelino, J., de Virginio Filho, E.M., Isaac, M.E., 2021. Shade tree traits and microclimate modifications: implications for pathogen management in biodiverse coffee agroforests. Biotropica 53, 1356–1367.

Gamon, J.A., Somers, B., Malenovský, Z., Middleton, E.M., Rascher, U., Schaepman, M. E., 2019. Assessing vegetation function with imaging spectroscopy. Surv. Geophys. 40, 489–513. https://doi.org/10.1007/s10712-019-09511-5.

Gascoin, S., Grizonnet, M., Bouchet, M., Salgues, G., Hagolle, O., 2019. Theia snow collection: high-resolution operational snow cover maps from Sentinel-2 and Landsat-8 data. Earth Syst. Sci. Data 11, 493–514. https://doi.org/10.5194/essd-11-493-2019.

Gitay, H.T., Noble, I.R., 1997. What are functional types and how should we seek them. Plant Funct. Types their Relev. Ecosyst. Prop. Glob. Change, 1, 3–19.

Gomarasca, U., Migliavacca, M., Kattge, J., Nelson, J.A., Niinemets, Ü., Wirth, C., Cescatti, A., Bahn, M., Nair, R., Acosta, A.T.R., Arain, M.A., Beloiu, M., Black, T.A., Bruun, H.H., Bucher, S.F., Buchmann, N., Byun, C., Carrara, A., Conte, A., da Silva, A.C., Duveiller, G., Fares, S., Ibrom, A., Knohl, A., Komac, B., Limousin, J.-M., Lusk, C.H., Mahecha, M.D., Martini, D., Minden, V., Montagnani, L., Mori, A.S., Onoda, Y., Peñuelas, J., Perez-Priego, O., Poschlod, P., Powell, T.L., Reich, P.B., Šigut, L., van Bodegom, P.M., Walther, S., Wohlfahrt, G., Wright, I.J., Reichstein, M., 2023. Leaf-level coordination principles propagate to the ecosystem scale. Nat. Commun. 14, 3948. https://doi.org/10.1038/s41467-023-39572-5.

Grabska, E., Frantz, D., Ostapowicz, K., 2020. Evaluation of machine learning algorithms for forest stand species mapping using Sentinel-2 imagery and environmental data in the polish Carpathians. Remote Sens. Environ. 251, 112103. https://doi.org/10.1016/j.rse.2020.112103.

Hansen, M.C., Potapov, P.V., Moore, R., Hancher, M., Turubanova, S.A., Tyukavina, A., Thau, D., Stehman, S.V., Goetz, S.J., Loveland, T.R., Kommareddy, A., Egorov, A., Chini, L., Justice, C.O., Townshend, J.R.G., 2013. High-resolution global maps of 21st-century forest cover change. Science 342, 850–853. https://doi.org/10.1126/science.1244693.

Haralick, R.M., Shanmugam, K., Dinstein, I., 1973. Textural features for image classification. IEEE Trans. Syst. Man Cybern. SMC-3, 610–621. https://doi.org/10.1109/TSMC.1973.4309314.

Hemmerling, J., Pflugmacher, D., Hostert, P., 2021. Mapping temperate forest tree species using dense Sentinel-2 time series. Remote Sens. Environ. 267, 112743. https://doi.org/10.1016/j.rse.2021.112743.

Hijmans, R.J., Cameron, S.E., Parra, J.L., Jones, P.G., Jarvis, A., 2005. Very high resolution interpolated climate surfaces for global land areas. Int. J. Climatol. 25, 1965–1978. https://doi.org/10.1002/joc.1276.

Huete, A.R., Liu, H.Q., Batchily, K., van Leeuwen, W., 1997. A comparison of vegetation indices over a global set of TM images for EOS-MODIS. Remote Sens. Environ. 59, 440–451. https://doi.org/10.1016/S0034-4257(96)00112-5.

Hunt, M.L., Blackburn, G.A., Carrasco, L., Redhead, J.W., Rowland, C.S., 2019. High resolution wheat yield mapping using Sentinel-2. Remote Sens. Environ. 233, 111410. https://doi.org/10.1016/j.rse.2019.111410.

IPBES, 2019. Summary for Policymakers of the Global Assessment Report on Biodiversity and Ecosystem Services. Zenodo. https://doi.org/10.5281/zenodo.3553579.

Jarvis, A., Guevara, E., Reuter, H.I., Nelson, A.D., 2008. Hole-Filled SRTM for the Globe : Version 4 : Data Grid.

Jetz, W., Cavender-Bares, J., Pavlick, R., Schimel, D., Davis, F.W., Asner, G.P., Guralnick, R., Kattge, J., Latimer, A.M., Moorcroft, P., Schaepman, M.E., Schildhauer, M.P., Schneider, F.D., Schrodt, F., Stahl, U., Ustin, S.L., 2016. Monitoring plant functional diversity from space. Nat. Plants 2, 1–5. https://doi.org/10.1038/NPLANTS.2016.24.

Joswig, J.S., Wirth, C., Schuman, M.C., Kattge, J., Reu, B., Wright, I.J., Sippel, S.D., Rüger, N., Richter, R., Schaepman, M.E., van Bodegom, P.M., Cornelissen, J.H.C.,

Díaz, S., Hattingh, W.N., Kramer, K., Lens, F., Niinemets, Ü., Reich, P.B., Reichstein, M., Römermann, C., Schrodt, F., Anand, M., Bahn, M., Byun, C., Campetella, G., Cerabolini, B.E.L., Craine, J.M., Gonzalez-Melo, A., Gutiérrez, A.G., He, T., Higuchi, P., Jactel, H., Kraft, N.J.B., Minden, V., Onipchenko, V., Peñuelas, J., Pillar, V.D., Sosinski, Ê., Soudzilovskaia, N.A., Weiher, E., Mahecha, M.D., 2022. Climatic and soil factors explain the two-dimensional spectrum of global plant trait variation. Nat. Ecol. Evol. 6, 36–50. https://doi.org/10.1038/s41559-021-01616-8.

Kampe, T.U., Johnson, B.R., Kuester, M.A., Keller, M., 2010. NEON: the first continental-scale ecological observatory with airborne remote sensing of vegetation canopy biochemistry and structure. J. Appl. Remote. Sens. 4 https://doi.org/10.1117/1.3361375, 043510.

Kattenborn, T., Lopatin, J., Förster, M., Braun, A.C., Fassnacht, F.E., 2019. UAV data as alternative to field sampling to map woody invasive species based on combined Sentinel-1 and Sentinel-2 data. Remote Sens. Environ. 227, 61–73. https://doi.org/10.1016/j.rse.2019.03.025.

Kattge, J., Bönisch, G., Díaz, S., Lavorel, S., Prentice, I.C., Leadley, P., Tautenhahn, S., Werner, G.D.A., Aakala, T., Abedi, M., Acosta, A.T.R., Adamidis, G.C., Adamson, K., Aiba, M., Albert, C.H., Alcántara, J.M., Alcázar, C.C., Aleixo, I., Ali, H., Amiaud, B., Ammer, C., Amoroso, M.M., Anand, M., Anderson, C., Anten, N., Antos, J., Apgaua, D.M.G., Ashman, T.L., Asmara, D.H., Asner, G.P., Aspinwall, M., Atkin, O., Aubin, I., Baastrup-Spohr, L., Bahalkeh, K., Bahn, M., Baker, T., Baker, W.J., Bakker, J.P., Baldocchi, D., Baltzer, J., Banerjee, A., Baranger, A., Barlow, J., Barneche, D.R., Baruch, Z., Bastianelli, D., Battles, J., Bauerle, W., Bauters, M., Bazzato, E., Beckmann, M., Beeckman, H., Beierkuhnlein, C., Bekker, R., Belfry, G., Belluau, M., Beloiu, M., Benavides, R., Benomar, L., Berdugo-Lattke, M.L., Berenguer, E., Bergamin, R., Bergmann, J., Bergmann Carlucci, M., Berner, L., Bernhardt-Römermann, M., Bigler, C., Bjorkman, A.D., Blackman, C., Blanco, C., Blonder, B., Blumenthal, D., Bocanegra-González, K.T., Boeckx, P., Bohlman, S., Böhning-Gaese, K., Boisvert-Marsh, L., Bond, W., Bond-Lamberty, B., Boom, A., Boonman, C.C.F., Bordin, K., Boughton, E.H., Boukili, V., Bowman, D.M.J.S., Bravo, S., Brendel, M.R., Broadley, M.R., Brown, K.A., Bruelheide, H., Brumnich, F., Bruun, H.H., Bruy, D., Buchanan, S.W., Bucher, S.F., Buchmann, N., Buitenwerf, R., Bunker, D.E., Bürger, J., Burrascano, S., Burslem, D.F.R.P., Butterfield, B.J., Byun, C., Marques, M., Scalon, M.C., Caccianiga, M., Cadotte, M., Cailleret, M., Camac, J., Camarero, J.J., Campany, C., Campetella, G., Campos, J.A., Cano-Arboleda, L., Canullo, R., Carbognani, M., Carvalho, F., Casanoves, F., Castagneyrol, B., Catford, J. A., Cavender-Bares, J., Cerabolini, B.E.L., Cervellini, M., Chacón-Madrigal, E., Chapin, K., Chapin, F.S., Chelli, S., Chen, S.C., Chen, A., Cherubini, P., Chianucci, F., Choat, B., Chung, K.S., Chytrý, M., Ciccarelli, D., Coll, L., Collins, C.G., Conti, L., Coomes, D., Cornelissen, J.H.C., Cornwell, W.K., Corona, P., Coyea, M., Craine, J., Craven, D., Cromsigt, J.P.G.M., Csecserits, A., Cufar, K., Cuntz, M., da Silva, A.C., Dahlin, K.M., Dainese, M., Dalke, I., Dalle Fratte, M., Dang-Le, A.T., Danihelka, J., Dannoura, M., Dawson, S., de Beer, A.J., De Frutos, A., De Long, J.R., Dechant, B., Delagrange, S., Delpierre, N., Derroire, G., Dias, A.S., Diaz-Toribio, M.H., Dimitrakopoulos, P.G., Dobrowolski, M., Doktor, D., Dřevojan, P., Dong, N., Dransfield, J., Dressler, S., Duarte, L., Ducouret, E., Dullinger, S., Durka, W., Duursma, R., Dymova, O., E-Vojtkó, A., Eckstein, R.L., Ejtehadi, H., Elser, J., Emilio, T., Engemann, K., Erfanian, M.B., Erfmeier, A., Esquivel-Muelbert, A., Esser, G., Estiarte, M., Domingues, T.F., Fagan, W.F., Fagúndez, J., Falster, D.S., Fan, Y., Fang, J., Farris, E., Fazlioglu, F., Feng, Y., Fernandez-Mendez, F., Ferrara, C., Ferreira, J., Fidelis, A., Finegan, B., Firn, J., Flowers, T.J., Flynn, D.F.B., Fontana, V., Forey, E., Forgiarini, C., François, L., Frangipani, M., Frank, D., Frenette-Dussault, C., Freschet, G.T., Fry, E.L., Fyllas, N.M., Mazzochini, G.G., Gachet, S., Gallagher, R., Ganade, G., Ganga, F., García-Palacios, P., Gargaglione, V., Garnier, E., Garrido, J.L., de Gasper, A.L., Gea-Izquierdo, G., Gibson, D., Gillison, A. N., Giroldo, A., Glasenhardt, M.C., Gleason, S., Gliesch, M., Goldberg, E., Göldel, B., Gonzalez-Akre, E., Gonzalez-Andujar, J.L., González-Melo, A., González-Robles, A., Graae, B.J., Granda, E., Graves, S., Green, W.A., Gregor, T., Gross, N., Guerin, G.R., Günther, A., Gutiérrez, A.G., Haddock, L., Haines, A., Hall, J., Hambuckers, A., Han, W., Harrison, S.P., Hattingh, W., Hawes, J.E., He, T., He, P., Heberling, J.M., Helm, A., Hempel, S., Hentschel, J., Hérault, B., Hereş, A.M., Herz, K., Heuertz, M., Hickler, T., Hietz, P., Higuchi, P., Hipp, A.L., Hirons, A., Hock, M., Hogan, J.A., Holl, K., Honnay, O., Hornstein, D., Hou, E., Hough-Snee, N., Hovstad, K.A., Ichie, T., Igić, B., Illa, E., Isaac, M., Ishihara, M., Ivanov, L., Ivanova, L., Iversen, C.M., Izquierdo, J., Jackson, R.B., Jackson, B., Jactel, H., Jagodzinski, A.M., Jandt, U., Jansen, S., Jenkins, T., Jentsch, A., Jespersen, J.R.P., Jiang, G.F., Johansen, J.L., Johnson, D., Jokela, E.J., Joly, C.A., Jordan, G.J., Joseph, G.S., Junaedi, D., Junker, R.R., Justes, E., Kabzems, R., Kane, J., Kaplan, Z., Kattenborn, T., Kavelenova, L., Kearsley, E., Kempel, A., Kenzo, T., Kerkhoff, A., Khalil, M.I., Kinlock, N.L., Kissling, W.D., Kitajima, K., Kitzberger, T., Kjøller, R., Klein, T., Kleyer, M., Klimešová, J., Klipel, J., Kloeppel, B., Klotz, S., Knops, J.M.H., Kohyama, T., Koike, F., Kollmann, J., Komac, B., Komatsu, K., König, C., Kraft, N.J. B., Kramer, K., Kreft, H., Kühn, I., Kumarathunge, D., Kuppler, J., Kurokawa, H., Kurosawa, Y., Kuyah, S., Laclau, J.P., Lafleur, B., Lallai, E., Lamb, E., Lamprecht, A., Larkin, D.J., Laughlin, D., Le Bagousse-Pinguet, Y., le Maire, G., le Roux, P.C., le Roux, E., Lee, T., Lens, F., Lewis, S.L., Lhotsky, B., Li, Y., Li, X., Lichstein, J.W., Liebergesell, M., Lim, J.Y., Lin, Y.S., Linares, J.C., Liu, C., Liu, D., Liu, U., Livingstone, S., Llusià, J., Lohbeck, M., López-García, Á., Lopez-Gonzalez, G., Lososová, Z., Louault, F., Lukács, B.A., Lukeš, P., Luo, Y., Lussu, M., Ma, S., Maciel Rabelo Pereira, C., Mack, M., Maire, V., Mäkelä, A., Mäkinen, H., Malhado, A.C.M., Mallik, A., Manning, P., Manzoni, S., Marchetti, Z., Marchino, L., Marcilio-Silva, V., Marcon, E., Marignani, M., Markesteijn, L., Martin, A., Martínez-Garza, C., Martínez-Vilalta, J., Mašková, T., Mason, K., Mason, N., Massad, T.J., Masse, J., Mayrose, I., McCarthy, J., McCormack, M.L., McCulloh, K., McFadden, I.R., McGill, B.J., McPartland, M.Y., Medeiros, J.S., Medlyn, B., Meerts, P., Mehrabi, Z., Meir, P., Melo, F.P.L., Mencuccini, M., Meredieu, C., Messier, J., Mészáros, I., Metsaranta, J., Michaletz, S.T., Michelaki, C., Migalina, S., Milla, R., Miller, J.E.D., Minden, V., Ming, R., Mokany, K., Moles, A.T., Molnár, A., Molofsky, J., Molz, M., Montgomery, R.A., Monty, A., Moravcová, L., Moreno-Martínez, A., Moretti, M., Mori, A.S., Mori, S., Morris, D., Morrison, J., Mucina, L., Mueller, S., Muir, C.D., Müller, S.C., Munoz, F., Myers-Smith, I.H., Myster, R.W., Nagano, M., Naidu, S., Narayanan, A., Natesan, B., Negoita, L., Nelson, A.S., Neuschulz, E.L., Ni, J., Niedrist, G., Nieto, J., Niinemets, Ü., Nolan, R., Nottebrock, H., Nouvellon, Y., Novakovskiy, A., Nystuen, K.O., O'Grady, A., O'Hara, K., O'Reilly-Nugent, A., Oakley, S., Oberhuber, W., Ohtsuka, T., Oliveira, R., Öllerer, K., Olson, M.E., Onipchenko, V., Onoda, Y., Onstein, R.E., Ordonez, J.C., Osada, N., Ostonen, I., Ottaviani, G., Otto, S., Overbeck, G.E., Ozinga, W.A., Pahl, A.T., Paine, C.E.T., Pakeman, R.J., Papageorgiou, A.C., Parfionova, E., Pärtel, M., Patacca, M., Paula, S., Paule, J., Pauli, H., Pausas, J.G., Peco, B., Penuelas, J., Perea, A., Peri, P.L., Petisco-Souza, A.C., Petraglia, A., Petritan, A.M., Phillips, O.L., Pierce, S., Pillar, V.D., Pisek, J., Pomogaybin, A., Poorter, H., Portsmuth, A., Poschlod, P., Potvin, C., Pounds, D., Powell, A.S., Power, S.A., Prinzing, A., Puglielli, G., Pyšek, P., Raevel, V., Rammig, A., Ransijn, J., Ray, C.A., Reich, P.B., Reichstein, M., Reid, D.E.B., Réjou-Méchain, M., de Dios, V.R., Ribeiro, S., Richardson, S., Riibak, K., Rillig, M.C., Riviera, F., Robert, E.M.R., Roberts, S., Robroek, B., Roddy, A., Rodrigues, A.V., Rogers, A., Rollinson, E., Rolo, V., Römermann, C., Ronzhina, D., Roscher, C., Rosell, J.A., Rosenfield, M.F., Rossi, C., Roy, D.B., Royer-Tardif, S., Rüger, N., Ruiz-Peinado, R., Rumpf, S.B., Rusch, G.M., Ryo, M., Sack, L., Saldaña, A., Salgado-Negret, B., Salguero-Gomez, R., Santa-Regina, I., Santacruz-García, A.C., Santos, J., Sardans, J., Schamp, B., Scherer-Lorenzen, M., Schleuning, M., Schmid, B., Schmidt, M., Schmitt, S., Schneider, J.V., Schowanek, S.D., Schrader, J., Schrodt, F., Schuldt, B., Schurr, F., Selaya Garvizu, G., Semchenko, M., Seymour, C., Sfair, J.C., Sharpe, J.M., Sheppard, C.S., Sheremetiev, S., Shiodera, S., Shipley, B., Shovon, T.A., Siebenkäs, A., Sierra, C., Silva, V., Silva, M., Sitzia, T., Sjöman, H., Slot, M., Smith, N. G., Sodhi, D., Soltis, P., Soltis, D., Somers, B., Sonnier, G., Sørensen, M.V., Sosinski, E. E., Soudzilovskaia, N.A., Souza, A.F., Spasojevic, M., Sperandii, M.G., Stan, A.B., Stegen, J., Steinbauer, K., Stephan, J.G., Sterck, F., Stojanovic, D.B., Strydom, T., Suarez, M.L., Svenning, J.C., Svitková, I., Svitok, M., Svoboda, M., Swaine, E., Swenson, N., Tabarelli, M., Takagi, K., Tappeiner, U., Tarifa, R., Tauugourdeau, S., Tavsanoglu, C., te Beest, M., Tedersoo, L., Thiffault, N., Thom, D., Thomas, E., Thompson, K., Thornton, P.E., Thuiller, W., Tichý, L., Tissue, D., Tjoelker, M.G., Tng, D.Y.P., Tobias, J., Török, P., Tarin, T., Torres-Ruiz, J.M., Tóthmérész, B., Treurnicht, M., Trivellone, V., Trolliet, F., Trotsiuk, V., Tsakalos, J.L., Tsiripidis, I., Tysklind, N., Umehara, T., Usoltsev, V., Vadeboncoeur, M., Vaezi, J., Valladares, F., Vamosi, J., van Bodegom, P.M., van Breugel, M., Van Cleemput, E., van de Weg, M., van der Merwe, S., van der Plas, F., van der Sande, M.T., van Kleunen, M., Van Meerbeek, K., Vanderwel, M., Vanselow, K.A., Vårhammar, A., Varone, L., Vasquez Valderrama, M.Y., Vassilev, K., Vellend, M., Veneklaas, E.J., Verbeeck, H., Verheyen, K., Vibrans, A., Vieira, I., Villacís, J., Violle, C., Vivek, P., Wagner, K., Waldram, M., Waldron, A., Walker, A.P., Waller, M., Walther, G., Wang, H., Wang, F., Wang, W., Watkins, H., Watkins, J., Weber, U., Weedon, J.T., Wei, L., Weigelt, P., Weiher, E., Wells, A.W., Wellstein, C., Wenk, E., Westoby, M., Westwood, A., White, P.J., Whitten, M., Williams, M., Winkler, D.E., Winter, K., Womack, C., Wright, I.J., Wright, S.J., Wright, J., Pinho, B.X., Ximenes, F., Yamada, T., Yamaji, K., Yanai, R., Yankov, N., Yguel, B., Zanini, K.J., Zanne, A.E., Zelený, D., Zhao, Y.P., Zheng, Jingming, Zheng, Ji, Ziemińska, K., Zirbel, C.R., Zizka, G., Zo-Bi, I.C., Zotz, G., Wirth, C., 2020. TRY plant trait database – enhanced coverage and open access. Glob. Chang. Biol. 26, 119–188. https://doi.org/10.1111/gcb.14904.

Kokaly, R.F., Skidmore, A.K., 2015. Plant phenolics and absorption features in vegetation reflectance spectra near 1.66μm. Int. J. Appl. Earth Obs. Geoinf. 43, 55–83. https://doi.org/10.1016/j.jag.2015.01.010. Special Issue on "Advances in remote sensing of vegetation function andtraits".

Kokaly, R.F., Asner, G.P., Ollinger, S.V., Martin, M.E., Wessman, C.A., 2009. Characterizing canopy biochemistry from imaging spectroscopy and its application to ecosystem studies. Remote Sens. Environ. 113, S78–S91. https://doi.org/10.1016/j.rse.2008.10.018.

Landry, M., Erlinger, T.P., Patschke, D., Varrichio, C., 2016. Probabilistic gradient boosting machines for GEFCom2014 wind forecasting. Int. J. Forecast. 32, 1061–1066. https://doi.org/10.1016/j.ijforecast.2016.02.002.

Lange, M., 2022. Mapping land-use intensity of grasslands in Germany with machine learning and Sentinel-2 time series. Remote Sens. Environ. 19.

Lavorel, S., McIntyre, S., Landsberg, J., Forbes, T.D.A., 1997. Plant functional classifications: from general groups to specific groups based on response to disturbance. Trends Ecol. Evol. 12, 474–478.

Liang, M., Baiser, B., Hallett, L.M., Hautier, Y., Jiang, L., Loreau, M., Record, S., Sokol, E. R., Zarnetske, P.L., Wang, S., 2022. Consistent stabilizing effects of plant diversity across spatial scales and climatic gradients. Nat. Ecol. Evol. 1–7 https://doi.org/10.1038/s41559-022-01868-y.

Liu, Y., Li, G., Wu, X., Niklas, K.J., Yang, Z., Sun, S., 2021. Linkage between species traits and plant phenology in an alpine meadow. Oecologia 195, 409–419. https://doi.org/10.1007/s00442-020-04846-y.

Liu, S., Yan, Z., Wang, Z., Serbin, S., Visser, M., Zeng, Y., Ryu, Y., Su, Y., Guo, Z., Song, G., Wu, Q., Zhang, H., Cheng, K.H., Dong, J., Hau, B.C.H., Zhao, P., Yang, X., Liu, L., Rogers, A., Wu, J., 2023. Mapping foliar photosynthetic capacity in sub-tropical and tropical forests with UAS-based imaging spectroscopy: scaling from leaf to canopy. Remote Sens. Environ. 293, 113612. https://doi.org/10.1016/j.rse.2023.113612.

Loozen, Y., Rebel, K.T., de Jong, S.M., Lu, M., Ollinger, S.V., Wassen, M.J., Karssenberg, D., 2020. Mapping canopy nitrogen in European forests using remote sensing and environmental variables with the random forests method. Remote Sens. Environ. 247, 111933. https://doi.org/10.1016/j.rse.2020.111933.

López, L.G.C., Medina, E.A.S., Peña, A.M., 2016. Effects of microclimate on species diversity and functional traits of corticolous lichens in the Popayan botanical garden (Cauca, Colombia). Cryptogam. Mycol. 37, 205–215.

Lundberg, S.M., Erion, G., Chen, H., DeGrave, A., Prutkin, J.M., Nair, B., Katz, R., Himmelfarb, J., Bansal, N., Lee, S.-I., 2020. From local explanations to global understanding with explainable AI for trees. Nat. Mach. Intell. 2, 56–67. https://doi.org/10.1038/s42256-019-0138-9.

Madani, N., Kimball, J.S., Ballantyne, A.P., Affleck, D.L.R., van Bodegom, P.M., Reich, P. B., Kattge, J., Sala, A., Nazeri, M., Jones, M.O., Zhao, M., Running, S.W., 2018. Future global productivity will be affected by plant trait response to climate. Sci. Rep. 8, 2870. https://doi.org/10.1038/s41598-018-21172-9.

Martin, M.E., Plourde, L.C., Ollinger, S.V., Smith, M.L., McNeil, B.E., 2008. A generalizable method for remote sensing of canopy nitrogen across a wide range of forest ecosystems. Remote Sens. Environ. 112, 3511–3519. https://doi.org/10.1016/j.rse.2008.04.008.

Martin, R.E., Dana Chadwick, K., Brodrick, P.G., Carranza-Jimenez, L., Vaughn, N.R., Asner, G.P., 2018. An approach for foliar trait retrieval from airborne imaging spectroscopy of tropical forests. Remote Sens. (Basel) 10. https://doi.org/10.3390/rs10020199.

Miraglio, T., Coops, N.C., Wallis, C.I.B., Crofts, A.L., Kalacska, M., Vellend, M., Serbin, S. P., Arroyo-Mora, J.P., Laliberté, E., 2023. Mapping canopy traits over Québec using airborne and spaceborne imaging spectroscopy. Sci. Rep. 13, 17179. https://doi.org/10.1038/s41598-023-44384-0.

Moreno-Martínez, Á., Camps-Valls, G., Kattge, J., Robinson, N., Reichstein, M., van Bodegom, P., Kramer, K., Cornelissen, J.H.C., Reich, P., Bahn, M., Niinemets, Ü., Peñuelas, J., Craine, J.M., Cerabolini, B.E.L., Minden, V., Laughlin, D.C., Sack, L., Allred, B., Baraloto, C., Byun, C., Soudzilovskaia, N.A., Running, S.W., 2018. A methodology to derive global maps of leaf traits using remote sensing and climate data. Remote Sens. Environ. 218, 69–88. https://doi.org/10.1016/j.rse.2018.09.006.

Myers-Smith, I.H., Thomas, H.J.D., Bjorkman, A.D., 2019. Plant traits inform predictions of tundra responses to global change. New Phytol. 221, 1742–1748. https://doi.org/10.1111/nph.15592.

Myneni, R.B., Hoffman, S., Knyazikhin, Y., Privette, J.L., Glassy, J., Tian, Y., Wang, Y., Song, X., Zhang, Y., Smith, G.R., Lotsch, A., Friedl, M., Morisette, J.T., Votava, P., Nemani, R.R., Running, S.W., 2002. Global products of vegetation leaf area and fraction absorbed PAR from year one of MODIS data. Remote Sens. Environ. 83, 214–231. https://doi.org/10.1016/S0034-4257(02)00074-3 the moderate resolution imaging Spectroradiometer (MODIS): a new generation of land surface monitoring.

Pacala, S., Kinzig, A.P., 2002. Introduction to theory and the common ecosystem model. In: Funct. Consequences Biodivers. Empir. Prog. Theor. Ext., pp. 169–174.

Poggio, L., de Sousa, L.M., Batjes, N.H., Heuvelink, G.B.M., Kempen, B., Ribeiro, E., Rossiter, D., 2021. SoilGrids 2.0: producing soil information for the globe with quantified spatial uncertainty. SOIL 7, 217–240. https://doi.org/10.5194/soil-7-217-2021.

Reich, P.B., 2012. Key canopy traits drive forest productivity. Proc. R. Soc. B Biol. Sci. 279, 2128–2134. https://doi.org/10.1098/rspb.2011.2270.

Reich, P.B., Walters, M.B., Ellsworth, D.S., 1997. From tropics to tundra: global convergence in plant functioning. Proc. Natl. Acad. Sci. 94, 13730–13734. https://doi.org/10.1073/pnas.94.25.13730.

Reichstein, M., Bahn, M., Mahecha, M.D., Kattge, J., Baldocchi, D.D., 2014. Linking plant and ecosystem functional biogeography. Proc. Natl. Acad. Sci. 111, 13697–13702. https://doi.org/10.1073/pnas.1216065111.

Richardson, A.D., 2019. Tracking seasonal rhythms of plants in diverse ecosystems with digital camera imagery. New Phytol. 222, 1742–1750. https://doi.org/10.1111/nph.15591.

Rogers, A., Medlyn, B.E., Dukes, J.S., Bonan, G., von Caemmerer, S., Dietze, M.C., Kattge, J., Leakey, A.D.B., Mercado, L.M., Niinemets, Ü., Prentice, I.C., Serbin, S.P., Sitch, S., Way, D.A., Zaehle, S., 2017. A roadmap for improving the representation of photosynthesis in earth system models. New Phytol. https://doi.org/10.1111/nph.14283.

Running, S.W., Loveland, T.R., Pierce, L.L., 1994. A vegetation classification logic-based on remote-sensing for use in global biogeochemical models. Ambio 23, 77–81.

Running, S.W., Loveland, T.R., Pierce, L.L., Nemani, R.R., Hunt, E.R., 1995. A remote sensing based vegetation classification logic for global land cover analysis. Remote Sens. Environ. 51, 39–48. https://doi.org/10.1016/0034-4257(94)00063-S. Remote Sensing of Land Surface for Studies of Global Chage.

Sanczuk, P., De Pauw, K., De Lombaerde, E., Luoto, M., Meeussen, C., Govaert, S., Vanneste, T., Depauw, L., Brunet, J., Cousins, S.A.O., Gasperini, C., Hedwall, P.-O., Iacopetti, G., Lenoir, J., Plue, J., Selvi, F., Spicher, F., Uria-Diez, J., Verheyen, K., Vangansbeke, P., De Frenne, P., 2023. Microclimate and forest density drive plant population dynamics under climate change. Nat. Clim. Chang. 1–8 https://doi.org/10.1038/s41558-023-01744-y.

Schiller, C., Schmidtlein, S., Boonman, C., Moreno-Martínez, A., Kattenborn, T., 2021. Deep learning and citizen science enable automated plant trait predictions from photographs. Sci. Rep. 11, 1–12. https://doi.org/10.1038/s41598-021-95616-0.

Schneider, F.D., Morsdorf, F., Schmid, B., Petchey, O.L., Hueni, A., Schimel, D.S., Schaepman, M.E., 2017. Mapping functional diversity from remotely sensed morphological and physiological forest traits. Nat. Commun. 8 https://doi.org/10.1038/s41467-017-01530-3.

Schneider, F.D., Longo, M., Paul-Limoges, E., Scholl, V.M., Schmid, B., Morsdorf, F., Pavlick, R.P., Schimel, D.S., Schaepman, M.E., Moorcroft, P.R., 2023. Remote sensing-based Forest modeling reveals positive effects of functional diversity on productivity at local spatial scale. J. Geophys. Res. Biogeosci. 128 https://doi.org/10.1029/2023JG007421 e2023JG007421.

Serbin, S.P., Wu, J., Ely, K.S., Kruger, E.L., Townsend, P.A., Meng, R., Wolfe, B.T., Chlus, A., Wang, Z., Rogers, A., 2019. From the Arctic to the tropics: multibiome prediction of leaf mass per area using leaf reflectance. New Phytol. 224, 1557–1568. https://doi.org/10.1111/nph.16123.

Singh, A., Serbin, S.P., McNeil, B.E., Kingdon, C.C., Townsend, P.A., 2015. Imaging spectroscopy algorithms for mapping canopy foliar chemical and morphological traits and their uncertainties. Ecol. Appl. 25, 2180–2197. https://doi.org/10.1890/14-2098.1.

Skidmore, A.K., Coops, N.C., Neinavaz, E., Ali, A., Schaepman, M.E., Paganini, M., Kissling, W.D., Vihervaara, P., Darvishzadeh, R., Feilhauer, H., Fernandez, M., Fernández, N., Gorelick, N., Geijzendorffer, I., Heiden, U., Heurich, M., Hobern, D., Holzwarth, S., Muller-Karger, F.E., Van De Kerchove, R., Lausch, A., Leitão, P.J., Lock, M.C., Mücher, C.A., O'Connor, B., Rocchini, D., Turner, W., Vis, J.K., Wang, T., Wegmann, M., Wingate, V., 2021. Priority list of biodiversity metrics to observe from space. Nat. Ecol. Evol. 5, 896–906. https://doi.org/10.1038/s41559-021-01451-x.

Sporbert, M., Jakubka, D., Bucher, S.F., Hensen, I., Freiberg, M., Heubach, K., König, A., Nordt, B., Plos, C., Blinova, I., Bonn, A., Knickmann, B., Koubek, T., Linstädter, A., Mašková, T., Primack, R.B., Rosche, C., Shah, M.A., Stevens, A., Tielbörger, K., Träger, S., Wirth, C., Römermann, C., 2022. Functional traits influence patterns in vegetative and reproductive plant phenology – a multi-botanical garden study. New Phytol. https://doi.org/10.1111/nph.18345 nph.18345.

Tilman, D., Isbell, F., Cowles, J.M., 2014. Biodiversity and ecosystem functioning. Annu. Rev. Ecol. Evol. Syst. 45, 471–493. https://doi.org/10.1146/annurev-ecolsys-120213-091917.

Ustin, S.L., Gamon, J.A., 2010. Remote sensing of plant functional types. New Phytol. 186, 795–816. https://doi.org/10.1111/j.1469-8137.2010.03284.x.

Ustin, S.L., Gitelson, A.A., Jacquemoud, S., Schaepman, M., Asner, G.P., Gamon, J.A., Zarco-Tejada, P., 2009. Retrieval of foliar information about plant pigment systems from high resolution spectroscopy. Remote Sens. Environ. 113, S67–S77. https://doi.org/10.1016/j.rse.2008.10.019.

Vallicrosa, H., Sardans, J., Maspons, J., Zuccarini, P., Fernández-Martínez, M., Bauters, M., Goll, D.S., Ciais, P., Obersteiner, M., Janssens, I.A., Peñuelas, J., 2022. Global maps and factors driving forest foliar elemental composition: the importance of evolutionary history. New Phytol. 233, 169–181. https://doi.org/10.1111/nph.17771.

van Bodegom, P.M., Douma, J.C., Verheijen, L.M., 2014. A fully traits-based approach to modeling global vegetation distribution. Proc. Natl. Acad. Sci. 111, 13733–13738. https://doi.org/10.1073/pnas.1304551110.

Vergopolan, N., Chaney, N.W., Pan, M., Sheffield, J., Beck, H.E., Ferguson, C.R., Torres-Rojas, L., Sadri, S., Wood, E.F., 2021. SMAP-HydroBlocks, a 30-m satellite-based soil moisture dataset for the conterminous US. Sci. Data 8, 264. https://doi.org/10.1038/s41597-021-01050-2.

Verrelst, J., Rivera, J.P., Gitelson, A., Delegido, J., Moreno, J., Camps-Valls, G., 2016. Spectral band selection for vegetation properties retrieval using Gaussian processes regression. Int. J. Appl. Earth Obs. Geoinf. 52, 554–567. https://doi.org/10.1016/j.jag.2016.07.016.

Violle, C., Navas, M.-L., Vile, D., Kazakou, E., Fortunel, C., Hummel, I., Garnier, E., 2007. Let the concept of trait be functional! Oikos 116, 882–892. https://doi.org/10.1111/j.2007.0030-1299.15559.x.

Walker, A.P., Quaife, T., van Bodegom, P.M., De Kauwe, M.G., Keenan, T.F., Joiner, J., Lomas, M.R., MacBean, N., Xu, C., Yang, X., Woodward, F.I., 2017. The impact of alternative trait-scaling hypotheses for the maximum photosynthetic carboxylation rate (Vcmax) on global gross primary production. New Phytol. 215, 1370–1386. https://doi.org/10.1111/nph.14623.

Wallis, C.I.B., Homeier, J., Peña, J., Brandl, R., Farwig, N., Bendix, J., 2019. Modeling tropical montane forest biomass, productivity and canopy traits with multispectral remote sensing data. Remote Sens. Environ. 225, 77–92. https://doi.org/10.1016/j.rse.2019.02.021.

Wang, Z., Chlus, A., Geygan, R., Ye, Z., Zheng, T., Singh, A., Couture, J.J., Cavender-Bares, J., Kruger, E.L., Townsend, P.A., 2020. Foliar functional traits from imaging spectroscopy across biomes in eastern North America. New Phytol. 228, 494–511. https://doi.org/10.1111/nph.16711.

Wang, Z., Townsend, P.A., Kruger, E.L., 2022. Leaf spectroscopy reveals divergent inter- and intra-species foliar trait covariation and trait–environment relationships across NEON domains. New Phytol. 235, 923–938. https://doi.org/10.1111/nph.18204.

Wessman, C.A., Aber, J.D., Peterson, D.L., Melillo, J.M., 1988. Remote sensing of canopy chemistry and nitrogen cycling in temperate forest ecosystems. Nature 335, 154–156. https://doi.org/10.1038/335154a0.

Whittaker, R.H., 1956. Vegetation of the Great Smoky Mountains. Ecol. Monogr. 26, 2–80. https://doi.org/10.2307/1943577.

Wieczynski, D.J., Díaz, S., Durán, S.M., Fyllas, N.M., Salinas, N., Martin, R.E., Shenkin, A., Silman, M.R., Asner, G.P., Bentley, L.P., Malhi, Y., Enquist, B.J., Savage, V.M., 2022. Improving landscape-scale productivity estimates by integrating trait-based models and remotely-sensed foliar-trait and canopy-structural data. Ecography. https://doi.org/10.1111/ecog.06078 e06078.

Wright, I.J., Reich, P.B., Westoby, M., Ackerly, D.D., Baruch, Z., Bongers, F., Cavender-Bares, J., Chapin, T., Cornellssen, J.H.C., Diemer, M., Flexas, J., Garnier, E., Groom, P.K., Gulias, J., Hikosaka, K., Lamont, B.B., Lee, T., Lee, W., Lusk, C., Midgley, J.J., Navas, M.L., Niinemets, Ü., Oleksyn, J., Osada, H., Poorter, H., Pool, P., Prior, L., Pyankov, V.I., Roumet, C., Thomas, S.C., Tjoelker, M.G., Veneklaas, E.J., Villar, R., 2004. The worldwide leaf economics spectrum. Nature 428. https://doi.org/10.1038/nature02403.

Wullschleger, S.D., Epstein, H.E., Box, E.O., Euskirchen, E.S., Goswami, S., Iversen, C.M., Kattge, J., Norby, R.J., van Bodegom, P.M., Xu, X., 2014. Plant functional types in earth system models: past experiences and future directions for application of dynamic vegetation models in high-latitude ecosystems. Ann. Bot. 114, 1–16.

Yan, Z., Sardans, J., Peñuelas, J., Detto, M., Smith, N.G., Wang, H., Guo, L., Hughes, A.C., Guo, Z., Lee, C.K.F., Liu, L., Wu, J., 2023. Global patterns and drivers of leaf photosynthetic capacity: the relative importance of environmental factors and evolutionary history. Glob. Ecol. Biogeogr. 32, 668–682. https://doi.org/10.1111/geb.13660.

Yin, G., Li, A., Wu, S., Fan, W., Zeng, Y., Yan, K., Xu, B., Li, J., Liu, Q., 2018. PLC: a simple and semi-physical topographic correction method for vegetation canopies based on path length correction. Remote Sens. Environ. 215, 184–198. https://doi.org/10.1016/j.rse.2018.06.009.

Zhao, Y., Lee, C.K.F., Wang, Z., Wang, J., Gu, Y., Xie, J., Law, Y.K., Song, G., Bonebrake, T.C., Yang, X., Nelson, B.W., Wu, J., 2022. Evaluating fine-scale phenology from PlanetScope satellites with ground observations across temperate forests in eastern North America. Remote Sens. Environ. 283, 113310. https://doi.org/10.1016/j.rse.2022.113310.

Update

Remote Sensing of Environment
Volume 307, Issue , 1 June 2024, Page

DOI: https://doi.org/10.1016/j.rse.2024.114171

Remote Sensing of Environment 307 (2024) 114171

Contents lists available at ScienceDirect

Remote Sensing of Environment

journal homepage: www.elsevier.com/locate/rse

Corrigendum to "Spectra-phenology integration for high-resolution, accurate, and scalable mapping of foliar functional traits using time-series Sentinel-2 data" [Remote Sensing of Environment 305 (2024) 114082]

Shuwen Liu [a], Zhihui Wang [b], Ziyu Lin [a], Yingyi Zhao [a], Zhengbing Yan [c], Kun Zhang [a], Marco Visser [d], Philip A. Townsend [e], Jin Wu [a,f,*]

[a] School of Biological Sciences, The University of Hong Kong, Pokfulam, Hong Kong, China
[b] Guangdong Provincial Key Laboratory of Remote Sensing and Geographical Information System, Guangdong Open Laboratory of Geospatial Information Technology and Application, Guangzhou Institute of Geography, Guangdong Academy of Sciences, Guangzhou 510070, China
[c] State Key Laboratory of Vegetation and Environmental Change, Institute of Botany, Chinese Academy of Sciences, Xiangshan, Beijing, China
[d] Institute of Environmental Sciences, Leiden University, Einsteinweg 2, 2333 CC Leiden, the Netherlands
[e] Department of Forest and Wildlife Ecology, University of Wisconsin-Madison, 1630 Linden Drive, Madison, WI 53706, USA
[f] Institute of Climate and Carbon Neutrality, The University of Hong Kong, Pokfulam, Hong Kong, China

The authors regret the previous absence of the results of the ENV + PFT models in the Fig. 6 of the article.

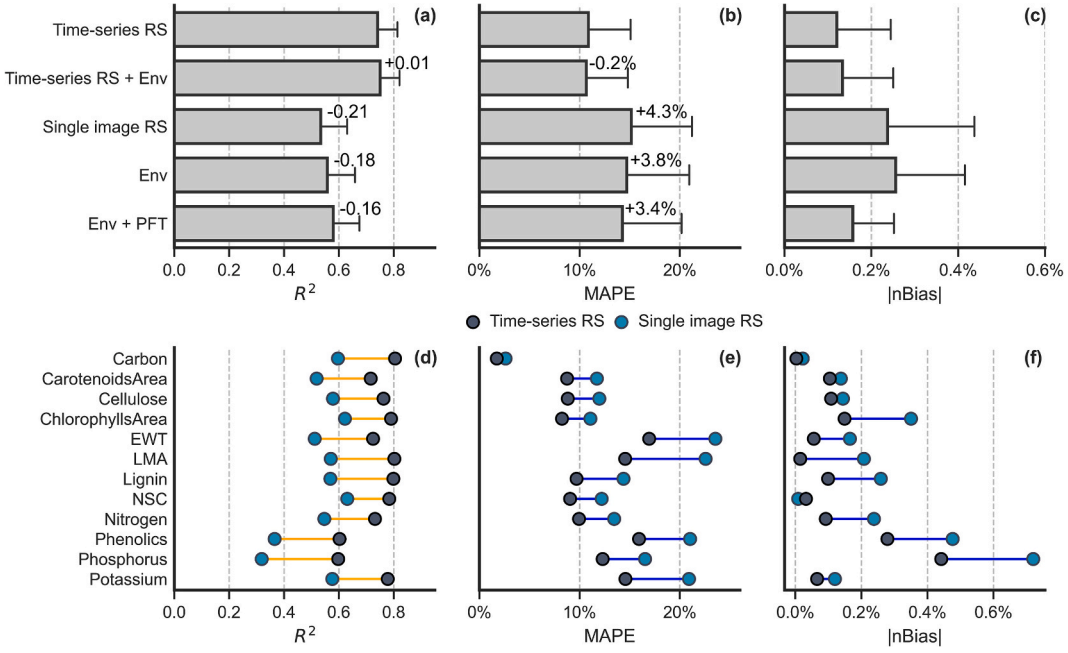

The authors would like to apologise for any inconvenience caused.

DOI of original article: https://doi.org/10.1016/j.rse.2024.114082.
* Corresponding author at: School of Biological Sciences, The University of Hong Kong, Pokfulam Road, Hong Kong, China.
E-mail address: jinwu@hku.hk (J. Wu).

https://doi.org/10.1016/j.rse.2024.114171

Available online 29 April 2024